# System Design of the Keck Planet Finder

Steven R. Gibson<sup>a</sup>, Andrew W. Howard<sup>a</sup>, Kodi Rider<sup>b</sup>, Samuel Halverson<sup>c</sup>, Arpita Roy<sup>d</sup>, Ashley D. Baker<sup>a</sup>, Jerry Edelstein<sup>b</sup>, Christopher Smith<sup>b</sup>, Benjamin J. Fulton<sup>a</sup>, Josh Walawender<sup>e</sup>, Max Brodheim<sup>e</sup>, Matthew Brown<sup>e</sup>, Dwight Chan<sup>e</sup>, Fei Dai<sup>f</sup>, William Deich<sup>g</sup>, Colby Gottschalk<sup>e</sup>, Jason Grillo<sup>b</sup>, David Hale<sup>a</sup>, Grant Hill<sup>e</sup>, Bradford Holden<sup>g</sup>, Aaron Householder<sup>h</sup>, Howard Isaacson<sup>i</sup>, Yuzo Ishikawa<sup>j</sup>, Sharon Jelinsky<sup>b</sup>, Marc Kassis<sup>e</sup>, Stephen Kaye<sup>a</sup>, Russ Laher<sup>a</sup>, Kyle Lanclos<sup>e</sup>, Chien-Hsiu Lee<sup>e</sup>, Scott Lilley<sup>e</sup>, Ben McCarney<sup>e</sup>, Timothy N. Miller<sup>b</sup>, Joel Payne<sup>e</sup>, Erik A. Petigura<sup>k</sup>, Claire Poppett<sup>b</sup>, Michael P. Raffanti<sup>b</sup>, Ryan Rubenzahl<sup>a</sup>, Dale Sanford<sup>g</sup>, Christian Schwab<sup>l</sup>, Abby P. Shaum<sup>a</sup>, Martin M. Sirk<sup>b</sup>, Roger Smith<sup>a</sup>, Jim Thorne<sup>e</sup>, John Valliant<sup>e</sup>, Adam Vandenberg<sup>e</sup>, Shin Ywan Wang<sup>a</sup>, Edward H. Wishnow<sup>b</sup>, Truman Wold<sup>e</sup>, Sherry Yeh<sup>e</sup>, Steve Baca<sup>e</sup>, Charles Beichman<sup>a</sup>, Bruce Berriman<sup>a</sup>, Thomas Brown<sup>e</sup>, Kelleen Casey<sup>e</sup>, Jason Chin<sup>e</sup>, James Chong<sup>e</sup>, David Cowley<sup>g</sup>, Mark Devenot<sup>e</sup>, Hamza Elwir<sup>e</sup>, Daniel Finstad<sup>b</sup>, Matthew Fraysse<sup>b</sup>, Ean James<sup>e</sup>, Elisha Jhoti<sup>k</sup>, Joe Killian<sup>e</sup>, Obie Levine<sup>e</sup>, Adela Chenyang Li<sup>h</sup>, Eduardo Marin<sup>e</sup>, Steve Milner<sup>e</sup>, Craig Nance<sup>e</sup>, Timothy J. O'Hanlon<sup>a</sup>, Daniel Orr<sup>e</sup>, Roberto Ortiz-Soto<sup>b</sup>, Tom Pavne<sup>b</sup>, Jacob Pember<sup>m</sup>, Gert Raskin<sup>m</sup>. Maureen Savage<sup>g</sup>, Andreas Seifahrt<sup>n</sup>, Brett Smith<sup>e</sup>, Rob Storesund<sup>e</sup>, Julian Stuermer<sup>o</sup>, Nick Suominen<sup>e</sup>, Jerez Tehero<sup>e</sup>, Tod Von Boeckmann<sup>e</sup>, Keith Wages<sup>e</sup>, Marie Weisfeiler<sup>p</sup>, Mavourneen Wilcox<sup>e</sup>, Peter Wizinowich<sup>e</sup>, and Anna Wolfenberger<sup>j</sup>

a California Institute of Technology, Pasadena, CA, United States
b Space Sciences Laboratory, University of California, Berkeley, CA, United States
c Jet Propulsion Laboratory, California Institute of Technology, Pasadena, CA, United States
d Astrophysics & Space Institute, Schmidt Sciences, New York, NY, United States
c W. M. Keck Observatory, Kamuela, HI, United States
f University of Hawaii, Manoa, HI, United States
g University of California Observatories, Santa Cruz, CA, United States
h Massachusetts Institute of Technology, Cambridge, MA, United States
i University of California, Berkeley, Berkeley, CA, United States
j Johns Hopkins University, Baltimore, MD, United States
k University of California, Los Angeles, CA, United States
Macquarie University, Sydney, Australia
m KU Leuven, Leuven, Belgium
n NOIRLab, Tucson, AZ, United States
c Heidelberg University, Heidelberg, Germany

<sup>p</sup>Desmarais LLP, Washington, DC, United States

## ABSTRACT

The Keck Planet Finder (KPF) is a fiber-fed, high-resolution, echelle spectrometer that specializes in the discovery and characterization of exoplanets using Doppler spectroscopy. In designing KPF, the guiding principles were high throughput to promote survey speed and access to faint targets, and high stability to keep uncalibrated systematic Doppler measurement errors below  $30\,\mathrm{cm\,s^{-1}}$ . KPF achieves optical illumination stability with a tip-tilt injection system, octagonal cross-section optical fibers, a double scrambler, and active fiber agitation. The optical bench and optics with integral mounts are made of Zerodur to provide thermo-mechanical stability. The spectrometer includes a slicer to reformat the optical input, green and red channels (445–600 nm and 600–870 nm), and achieves a resolving power of ~97,000. Additional subsystems include a separate, medium-resolution UV spectrometer (383–402 nm) to record the Ca II H & K lines, an exposure meter for real-time flux monitoring, a solar feed for sunlight injection, and a calibration system with a laser frequency comb and etalon for wavelength calibration. KPF was installed and commissioned at the W. M. Keck Observatory in late 2022 and early 2023 and is now in regular use for scientific observations. This paper presents an overview of the as-built KPF instrument and its subsystems, design considerations, and initial on-sky performance.

Keywords: Spectrometer, exoplanets, Doppler spectroscopy, radial velocity, Zerodur

## 1. INTRODUCTION

The Keck Planet Finder (KPF) is a fiber-fed, high-resolution, high-stability spectrometer specifically designed to characterize exoplanets using Doppler spectroscopy. The instrument includes a green channel (445–600 nm) and a red channel (600–870 nm), and achieves a resolving power of ~97,000 and a Doppler precision of less than  $30\,\mathrm{cm\,s^{-1}}$ . KPF was installed at the W. M. Keck Observatory (WMKO) in late 2022 and, after a short commissioning period, is now making routine science observations. KPF joins a stable of recently commissioned extreme precision radial velocity (EPRV) facilities that aim to reach 10's of cm s<sup>-1</sup> performance.<sup>1–5</sup> These facilities span a range of design philosophies and technical implementations, but share a common goal of pushing measurement capabilities to the level required to detect Earth-mass planets. This goal is a central priority in the exoplanet community, both as a stand-alone science pursuit and as a key step in supporting a future space-borne direct imaging mission that will record images and atmospheric spectra of nearby exo-Earths.<sup>6</sup>

Several institutions contributed to the KPF project: the Space Sciences Laboratory (SSL) at UC Berkeley was the primary design and build location; the California Institute of Technology (Caltech) developed the data reduction pipeline, designed the CCD electronics and characterized the detectors; designed, aligned, and tested the Calcium H & K spectrometer; and also designed and built the Solar Calibrator; WMKO was responsible for the fiber injection unit (FIU) and facility-related interfaces; the University of California Observatories (UCO) developed and wrote the instrument control software and also helped with detector selection; and Macquarie University developed the Fabry-Pérot etalon for the KPF calibration system.

This paper provides an overview of the entire as-built KPF system. It updates our 2018 SPIE paper,<sup>7</sup> which described the design just after the project's preliminary design review. During the intervening years, various subsystems have also been documented in more detail in other papers, such as the Fiber Injection Unit,<sup>8</sup> Calcium H&K spectrometer,<sup>9</sup> main spectrometer opto-mechanical design,<sup>10</sup> optical fiber testing and performance,<sup>11</sup> and the main spectrometer optical design, Zerodur bench, data reduction pipeline, fiber agitator, fiber cables, scramblers, VPH gratings, and exposure meter.<sup>12</sup>

## 2. KPF SCIENCE

KPF was designed to discover and characterize extrasolar planets using Doppler measurements from high-resolution optical spectra of stars. These measurements detect the star being pulled by its planets around the center of mass of the planetary system, causing the star's velocity to vary. The component of the velocity along the line of sight—the radial velocity (RV)—can be detected as a Doppler shift in the star's spectrum. Planet properties, including mass and orbital parameters, can be inferred by fitting a time series of these RV measurements. KPF is designed to achieve high Doppler precision (small Doppler errors) so that it can measure signals induced by small planets. Paired with Keck, KPF can access faint targets, take very high signal-to-noise

spectra of bright stars, and conduct large-scale surveys with limited nights. These features will allow KPF to address important questions in several areas of exoplanet science and astronomy broadly, including:

- Small planets around nearby stars: KPF will search the nearest stars for planets in the Earth-mass regime. These discoveries will teach us about the formation and evolution of planets like our own and will be the best targets for future ground-based and space-borne direct imaging observations. Nearby stars will also allow KPF to achieve its full potential and explore the realm of high signal-to-noise (SNR) spectra over a wide spectral bandwidth. KPF will be sensitive to close-in Earths, super-Earths, and sub-Neptunes (>1 Earth-mass planets in 0.1 AU orbits) for nearby, quiet stars. Although these types of planets are among the most interesting and well-studied from the Kepler mission, 13,14 the census of such small planets around nearby Sun-like stars is far from complete. Independently detecting and studying the mass distribution of small planets, many of which will not transit, in the Solar neighborhood will lead to insights about their formation, evolution, and diversity. Extremely high (>1000) SNR will allow KPF to discern subtle stellar line asymmetries to new levels. Close monitoring of these targets will reveal residual systematics from instrumental and astrophysical sources and inform the path to extreme precision (<10 cm s<sup>-1</sup>), either with upgrades to KPF or successor instruments. In addition to "Sun-like" G and K dwarfs, KPF will observe M dwarfs that are attractive because a planet in the habitable zone would have a small orbit (0.07–0.3 AU), boosting the amplitude of a signal of an Earth-mass planet to  $\sim 1\,\mathrm{m\,s^{-1}}$ . KPF's bandpass includes the 700–900 nm sweet spot<sup>15</sup> of maximal Doppler information content for M dwarfs.
- Transiting planets: Measuring masses of transiting planets using RVs is crucial for constraining planet composition via bulk density. KPF will play an central role in measuring planet masses at high precision, exploring the diverse population of super-Earths/sub-Neptunes with discoveries from TESS and Kepler. Precise masses are also critical to interpreting atmospheric features in planetary spectra<sup>16</sup> since the depths of most absorption features are proportional to the atmospheric scale height—a quantity computed from mass (surface gravity) and composition (atmospheric mean molecular weight), which are otherwise degenerate. Followup of Kepler planets offers special opportunities because most of the 4,000 planets discovered based on photometry from that mission are inaccessible to the previous generation of RV facilities due to lack of aperture and/or sufficient Doppler precision. This has led to the unfortunate situation in which we have thousands of exoplanetary systems with a fascinating variety of architectures, hundreds of which have multiple transiting planets and exhibit information-rich patterns of transit-timing variations (TTVs), dozens of which are temperate planets around Sun-like stars of a type that will not be found with TESS — but until now we have not been able to measure their masses. Leveraging the 10 m Keck aperture and KPF's efficient optical train, the system will enable detailed studies of the rich population of small planets from Kepler. KPF will also play important roles in future missions that study transiting planets, including PLATO and Ariel.
- Obliquities: The stellar obliquity the angle between a star's spin axis and the orbital axis of a planet is a tracer of the dynamical history of a planetary system, similar to the orbital eccentricity. The most direct method for measuring a star's obliquity is to detect the Rossiter-McLaughlin (RM) effect, the perturbation of a star's spectral lines during a planetary transit. The hosts of hot Jupiters have a broad distribution of obliquities, ranging from well-aligned systems to others that show polar or retrograde orbits. However, almost all previous measurements have involved hot Jupiters around FGK stars. Advancements in obliquity studies have been slow over the past decade because of the difficulty of performing RM observations of smaller planets and cooler stars. KPF will expand the domain of obliquity measurements to include small planets, M dwarf planets, and multi-planet systems by delivering high-SNR observations in the 5–10 minute exposures that are required to adequately sample RM signals (both in bulk RV and in line-profile change measurements) across a wide range of host star spectral types.
- Planetary atmospheres: Properties of the atmospheres of exoplanets can also be measured during transits. High-resolution optical ground-based spectroscopy now regularly makes atmospheric measurements of transiting extrasolar planets via phase-resolved (R > 20,000) spectroscopy. Thermal emission is sensitive to the vertical temperature structure and molecular/elemental abundance ratios on the planet's day side,

while transmission spectroscopy (accessible for a broader range of planets) complements the thermal measurements by probing higher altitudes in the atmosphere and measuring abundances, temperatures, and even wind speeds. At R > 90,000, the contrast of spectral features increases significantly, and individual atmospheric species become detectable.<sup>19</sup> With its combination of resolution and aperture, KPF will be a premier optical instrument for making such measurements in the Northern hemisphere, opening a new window into atmospheric studies of nearby planets.

• Asteroseismology: Stellar oscillations are a probe of the interior structure of stars, with frequencies and amplitudes that depend on age, mass, and radius. Early RV results were limited to only a few stars due to lack of precision and collecting area. More recently, the space-based photometry from CoRoT, Kepler, and TESS has revolutionized asteroseismology, with breakthroughs in understanding the internal structure and rotation of stars, <sup>20</sup> including stars with detected planets. <sup>21</sup> However, cool dwarfs are an unexplored frontier, largely inaccessible to photometry due to the small amplitudes of the corresponding photometric variations. Such stars are ubiquitous, yet our understanding of their structure remains one of the most challenging problems in stellar astrophysics. Models frequently underestimate radii of K and M dwarfs relative to observations. <sup>22</sup> This is especially pertinent because these stars are prime targets for exoplanet science with TESS and JWST. KPF's uniquely fast Doppler 'speed', combined with low instrumental systematics floor, will allow for an unparalleled view into the asteroseismic signals of nearby dwarf stars.

#### 3. SYSTEM OVERVIEW

## 3.1 System Design Philosophy

Designing a high-precision Doppler spectrometer for one of the 10 m Keck telescopes presented the opportunity to consider how aspects of the system architecture could be optimized for the science-driven goals of high optical throughput and high Doppler precision. KPF is not the first instrument of this type, and the landscape provides many instrument designs to consider. Some architectural features appear to have reached a point of evolutionary optimum (e.g., the basic architecture of a white pupil echelle spectrometer), and for these system elements our approach was to optimize the details given the facility constraints and top-level goals, not rethink the overall design philosophy. But for many other architectural features, we found that system performance is significantly impacted by the size and layout of the WMKO facility, and were worth rethinking. In this section, we briefly describe the top-level system design choices for KPF and their motivations.

The large aperture of a 10 m telescope uniquely enables observations of faint targets, high signal-to-noise spectra of bright targets, and the execution of surveys with large numbers of targets. To further accentuate KPF's strength in this area, we optimized the system design for high efficiency. This included prioritizing a high-efficiency optical train through the choice of efficient coatings with a minimum number of optical elements. We selected a relatively large optical fiber (225  $\mu$ m diameter = 1.14" on sky, relative to a median observatory seeing of 0.7") to capture as much stellar flux as practical. The large fiber size, combined with the large primary mirror diameter, meant that we needed an optical slicer/reformatter to keep the spectrometer size and cost reasonable for a resolving power of ~100,000. (Note that the KPF spectrometer (3× slicing) is comparable in size to 'unsliced' precision RV instruments on 3-4m telescopes, in spite of Keck I being about 3× the diameter).

The layout of the W. M. Keck Observatory necessitated a long fiber to traverse the telescope structure and terminate in the more stable basement environment. The transmission losses for a  $\sim$ 60 m fiber were most significant in at blue wavelengths, which led to our bandpass choice of 445–870 nm, which captures the astrophysically-important Ca II infrared triplet lines in the red and goes as blue as is practical given transmission loss and spectrum formatting on the detectors. This choice captures much of the Doppler information content for G, K, and M type dwarf stars. It misses the Ca II H & K lines in the near-UV that are important for monitoring stellar activity, which led to the addition of a separate dedicated medium-resolution spectrometer with a short fiber run for that purpose.

The need for high Doppler stability drove our emphasis on thermal, mechanical, and optical stability. The most noteworthy choice was to build as much of the main spectrometer as possible out of Zerodur glass, leveraging its exquisitely athermal properties. Building precision three-dimensional structures out of Zerodur is novel in astronomical instrumentation so we built a series of test units to demonstrate aspects of the design. It is

difficult to build cameras with transmissive optics and barrel-shaped support structures out of Zerodur, so we athermalized those designs as much as possible using standard material mixtures. The instrument illumination system needs to be stabilized as well such that the near field and far field of the beam that enters the spectrometer is nearly independent of the illumination of the optical fiber in the telescope's focal plane. This drove us to use a double scrambler and octagonal optical fibers to perform image "scrambling", a mechanical fiber agitator to gently shake the fiber cables and homogeneously mix the otherwise static fiber spatial modes, and a fast tip-tilt system to keep the star's image centered on the fiber tip at the telescope injection.

High Doppler stability also implies the ability to precisely measure and track the wavelength of each CCD pixel, which we achieve through a calibration system that includes a laser frequency comb and a highly regimented calibration schedule. The information from these spectra is captured by a data reduction pipeline that produces publication-ready data products to non-expert users and tracks the instrument state to sense and correct for instrument changes.

## 3.2 Top-level Design

The top-level requirements for KPF were high throughput to promote survey speed and access to faint targets and high stability to keep uncalibrated systematic Doppler measurement errors below  $50 \,\mathrm{cm} \,\mathrm{s}^{-1}$  (with a goal of  $30 \,\mathrm{cm} \,\mathrm{s}^{-1}$ ). To ensure the instrument met the high throughput requirement, during development the expected asbuilt throughput was estimated with an efficiency model (to be described more in Section 6.2). Throughout this paper, design variables chosen to maximize throughput are discussed, including optical designs, optical coatings, fiber lengths, and detector quantum efficiencies. To ensure that the instrument met the stability requirement, the team employed a Doppler-precision error budget to track the contributions of the various subsystems.<sup>7,24</sup> A top-level summary of the final error budget is shown in Figure 1.

KPF was designed from the start as an EPRV instrument, and as such the Doppler stability requirement was the primary driver for the design. To achieve this level of stability, KPF is comprised of several subsystems (Figure 2), each with an important role to play towards maximizing stability. These subsystems fall into several categories, which will be described within the following sections: the spectrometer optical design; illumination stability; mechanical and environmental stability; calibration; ancillary measurements (for barycentric correction and stellar activity monitoring), and software (for instrument control and data reduction).

## 3.3 Spectrometer Optical Design

The convergence of the radial velocity community on the white pupil spectrometer design is evident by a survey of existing or planned EPRV instruments based on the design: CARMENES, <sup>26</sup> ESPRESSO, <sup>1</sup> EXPRES, <sup>2</sup> G-CLEF, <sup>27</sup> HARPS, <sup>28</sup> HARPS-N, <sup>4</sup> HPF, <sup>29</sup> MAROON-X, <sup>5</sup> NEID, <sup>3</sup> and PARAS. <sup>30</sup>

The KPF spectrometer optical design is shown in Figure 3, with a summary of various parameters provided in Table 1. Light enters the core spectrometer following the image-slicing reformatter (see Section 3.5.1), at the focal point of the primary collimator mirror (traditionally, this would be the location of the spectrometer slit). The f/8 beam diverges past this point and then strikes the primary collimator mirror (an off-axis paraboloid). Upon reflection, the now collimated 200 mm diameter light beam travels to the echelle grating, located one

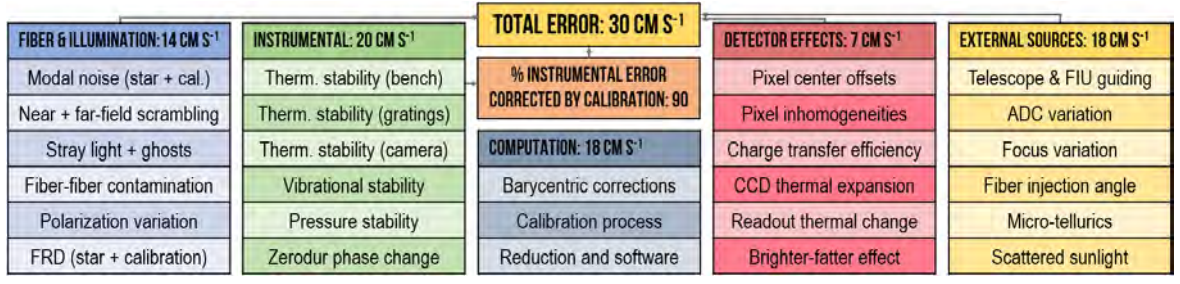


Figure 1. Major components in the KPF Doppler error budget. Individual error terms are categorized by type, with some fraction considered 'calibratable' (tracked by the simultaneous calibration channel) and others not. This follows similar system-level analyses from other EPRV facilities.<sup>2,24,25</sup>

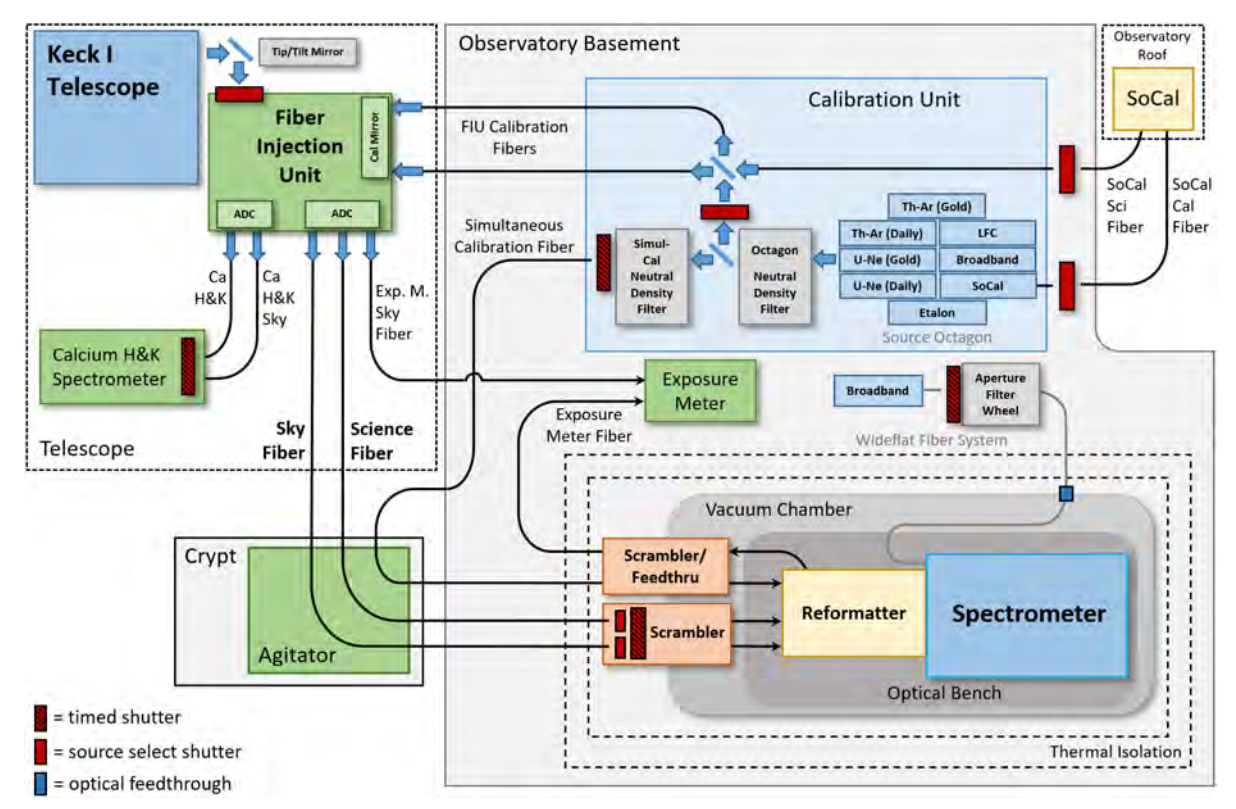


Figure 2. Schematic overview of the KPF system. The fiber injection unit and Calcium H&K spectrometer are located on the telescope's Nasmyth platform. The main spectrometer, calibration unit and exposure meter are located within the observatory basement. The fiber agitator (for modal noise suppression) is located in the "crypt", which is a small room directly underneath the azimuth axis of the telescope, connecting the dome and the coudé tunnel to the observatory basement. The Solar Calibrator (SoCal) is located on the roof of the observatory between the Keck I and Keck II domes.

primary collimator focal length away from the primary collimator. After diffraction by the echelle, the diverging bundle of collimated monochromatic beams reflect from the primary collimator a second time. Because the echelle grating is rotated slightly out of plane (the echelle gamma angle), the dispersed light does not return along the same path, and the pre- and post-diffraction beams are separated. Therefore, after reflecting from the collimator the second time, the dispersed light does not return to the entrance slit, but forms an intermediate focus to the side of the echelle. Just before the intermediate focus, a flat mirror is employed to fold the beam, to make the spectrometer footprint more compact.

After the fold mirror reflection, the light rays go through the intermediate focus, and then the diverging monochromatic beams are collimated by the secondary collimator mirror (an off-axis paraboloid). The monochromatic beam diameter here is  $160 \,\mathrm{mm}$ , owing to the secondary collimator having a focal length  $0.8\times$  that of the primary collimator (determined via a trade study in the conceptual design phase<sup>31</sup>). The converging, collimated monochromatic beams next encounter a dichroic beamsplitter, which reflects the green bandpass and transmits the red.

After reflection, the green channel monochromatic beams continue to converge towards the white pupil, with the cross-dispersion grism (grating-prism) located just beyond that point. This disperser consists of a shallow apex angle fused-silica prism bonded to a volume phase holographic (VPH) grating (with fused-silica cover plates). Following the grism, the light enters the camera, which then focuses the spectrum onto the CCD detector. The red channel monochromatic beams are transmitted through the dichroic, and are reflected by the red fold mirror (to steer the beam back on to the footprint of the optical bench), after which they also travel through a cross-dispersing grism and camera.

The grisms are yawed at an angle to the optical axes of the cameras (3.9° for the green and 4.8° for the red),

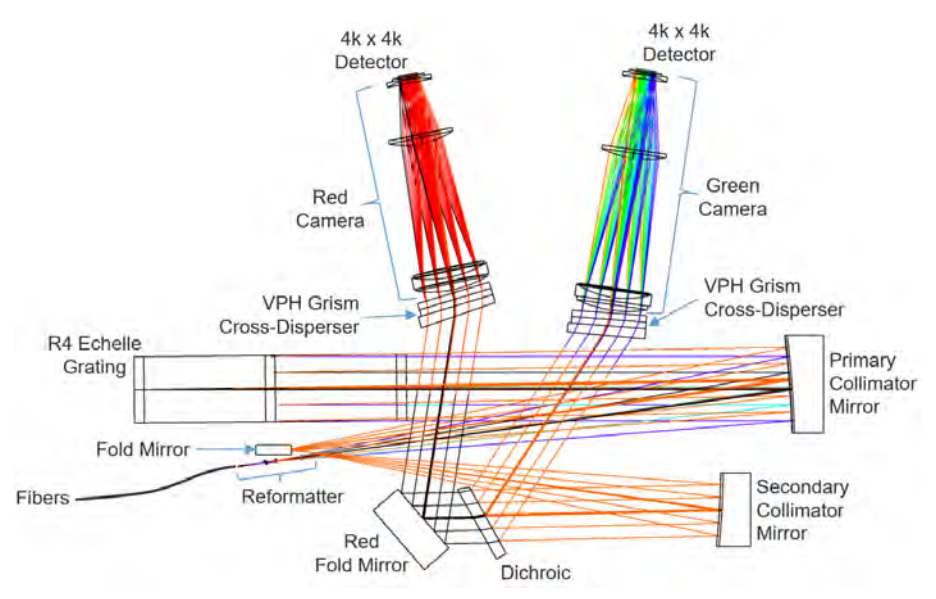


Figure 3. The final optical layout of the KPF spectrometer.

to steer a ghost path (between the CCD and the VPH rear surface) away from the detector. Both the prisms and the VPH gratings are square in outline, which aided alignment during both the grating fabrication and the prism-grating bonding processes.

Both the green and red cameras are five-element Petzval designs (Figure 4), consisting of a bonded triplet, followed by a singlet lens, and finally a field flattener lens just before the CCD detector. Both the green and red cameras use the same glass types with the exception of the L4 lens. The first surface of the triplet is a convex even asphere, and the final surface of the field flattener is a convex cylinder. The elements in both cameras are of similar sizes, which allows for many common opto-mechanical assemblies between the two channels.

Winlight Systems finalized the optical design of the KPF cameras, and designed the opto-mechanics for the cameras. Winlight also fabricated the optics and mechanics, and assembled and aligned both cameras. As shown in Figure 5, the grism cell was incorporated into the front of the camera barrel assembly. This simplified the grism cell designs (compared to alternatives interfacing with the bench), and also allowed the grisms to provide a counterweight to the cryostats mounted at the other end of the camera barrel. As such, this helped to balance the completed assembly, which was mounted at its center of mass within a fork-style mount.

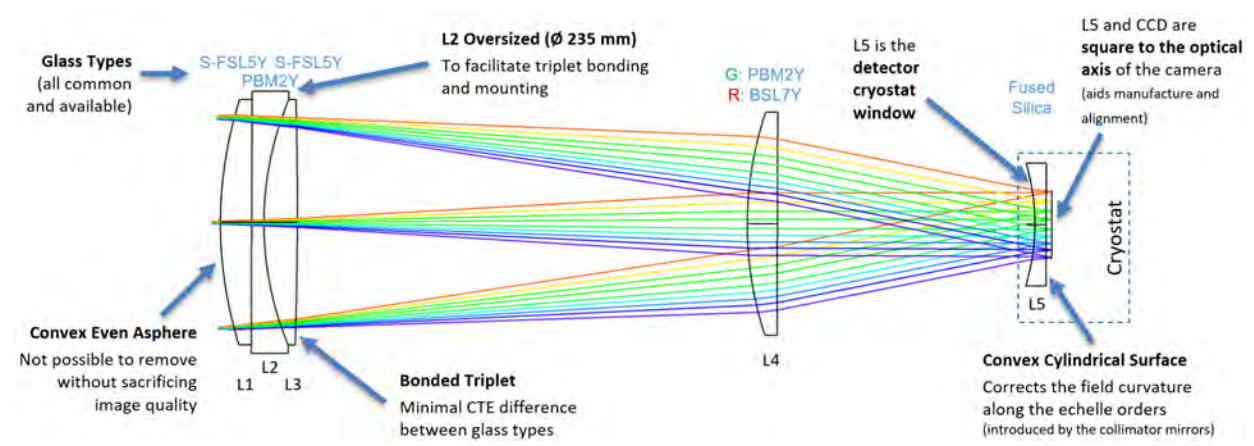


Figure 4. The green channel camera design. This meridional view is in the cross-dispersion direction, with the blaze wavelengths of five echelle orders shown. The red channel design is very similar (the only differences being the L4 glass type, surface curvatures, spacings and aspheric coefficients).

Table 1. Summary table of main spectrometer nominal parameters.

Parameter	Value
Optical design family	Asymmetric white pupil
Collimated beam diameter	200 mm
Collimator f/number	f/8
Asymmetric ratio	0.8
Resolving power	~98,000
Resolution element sampling	3 to 4 pixels (echelle dispersion direction)
Source fiber details	Science: $225\mu\mathrm{m}$ octagonal Sky: $225\mu\mathrm{m}$ octagonal, masked to $64\mu\mathrm{m}$ wide Simultaneous calibration: $120\mu\mathrm{m}$ octagonal, masked to $64\mu\mathrm{m} \times 64\mu\mathrm{m}$
Primary Collimator	Off-axis paraboloid 1600 mm focal length, f/8 beam Substrate: $456 \mathrm{mm}$ tall $\times$ 302 mm wide (112 mm thick) Decenter: $237 \mathrm{mm}$
Primary disperser	R4 ( $\theta_B = 75.96^\circ$ ) echelle mosaic Master: Richardson MR263 31.6 grooves per mm Substrate: 840 mm × 214 mm × 125 mm
Secondary Collimator	Off-axis paraboloid 1280 mm focal length, f/8 beam Substrate: $432 \mathrm{mm}$ tall $\times$ 230 mm wide (100 mm thick) Decenter: $149 \mathrm{mm}$
Dichroic	Transition wavelength: $590\mathrm{nm}$ Substrate: $415\mathrm{mm}$ tall $\times$ $246\mathrm{mm}$ wide ( $35\mathrm{mm}$ thick) Wedge: $0.5^\circ$
Wavelength coverage	Green channel: 443 nm to 599 nm Red channel: 599 nm to 871 nm
Cross-dispersers	VPH grisms Green VPH: 810 lines per mm Red VPH: 450 lines per mm
Green Camera	Focal Length: 495 mm, f/2.8 Largest camera lens: 235 mm diameter
Red Camera	Focal Length: 492 mm, f/2.8 Largest camera lens: 235 mm diameter
Detectors (Green and Red)	$4080 \times 4080$ pixels, $15 \mu\mathrm{m}$ -square pixels

# 3.3.1 Detectors

Both of the KPF detectors are  $4080 \times 4080$ -pixel devices, with 15  $\mu$ m-square pixels. With today's larger CCD sizes, this smaller size was a deliberate choice to minimize the effects of CCD expansion and contraction. For both channels, we chose STA4850 devices from Semiconductor Technology Associates (STA), which are mounted in a package designed specifically for thermal and mechanical stability. A 30  $\mu$ m-thick version of the STA4850 with a "mid-band" AR coating provided the best option for the KPF green arm. For the red arm (where fringing is more of a concern), we initially considered a 100  $\mu$ m-thick device, but after a detailed, EPRV-focused trade study, we decided on a 30  $\mu$ m-thick version with the red-tuned "LSST" AR coating. As such, aside from the

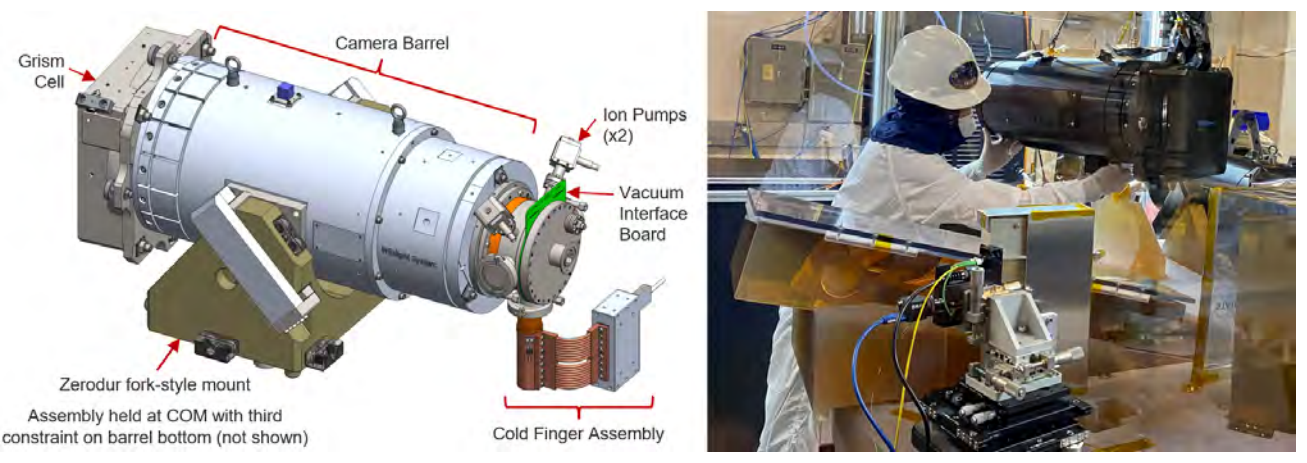


Figure 5. Left: Details of the KPF camera assembly. Right: The red camera assembly, supported by a crane during installation within the spectrometer. Also note in the foreground a Point Source Microscope (PSM) mounted on a multi-axis stage, which proved invaluable as a reformatter proxy during the early stages of spectrometer alignment.

coatings, both CCDs are the same and both channels share the same cryostat designs. Both channels utilize STA "Archon AC" CCD controllers with "HeaterX" boards within to control heaters in the CCD cooling system. We note that we plan to transition the heaters away from the Archons to dedicated Lakeshore controllers. This will allow the two systems to operate independently (allowing thermal stability to be maintained even if the Archons are taken off-line).

The design, build and test of the detector cryostats was a multi-institutional effort. CCD selection was supported by UCO. The cryostat mechanics and cold fingers were designed and built at SSL. The cryostat on-board electronics (and vacuum-interface PCB board, which brings the CCD electrical signals outside of the vacuum cryostat) were designed by Caltech. Once the cryostats were assembled at SSL, they were sent to Caltech for testing and characterizing of the entire system (consisting of CCD, electronics, and controllers).

## 3.3.2 Spectral Formats

The spectral formats of the green and red channels, accompanied by actual KPF spectra, are shown in Figure 6. The green spectral format was set so that the sodium doublet was placed one order inwards from the red edge of the green CCD. In addition, the start of the dichroic transition region (demarcated by the 95% throughput point) was set just redward of the sodium doublet at 590 nm, to ensure these lines do not fall within the reduced throughput region of the dichroic crossover region. The bluest order on the red CCD was set to provide continuous wavelength coverage between the two channels. At the red end, the Ca IR triplet lines are located just inside the red end of the red CCD (these are astrophysically-important lines that can be utilized as stellar activity indicators). To prevent cross-talk, another important consideration was to ensure a gap of at least 4 pixels existed between the "orderlets" within each order (see Section 3.5.1), and between the two bluest orders on each CCD.

Care was taken to square the orders and the resolution elements to the CCD rows and columns (on average). Squaring the orders to the CCD (by rotating the CCD) helps simplify the extraction of spectra in the data reduction pipeline, and squaring the resolution elements with the CCD (by rotating the slit, or in the KPF case the entire reformatter) avoids the resolution-smearing effects of line tilt. As such, the green CCD is clocked 2.44°, the red CCD is clocked 1.91°, and the reformatter is clocked 2.13°. Both CCDs were also translated 3 mm in the echelle-dispersion direction to better-center the spectral formats on the CCDs.

#### 3.4 Illumination Stability

Stable illumination of the spectrometer is paramount for an EPRV instrument, as any changes of the light distribution in either the image or pupil planes can cause displacements of the spectrum that closely mimic Doppler shifts. This section describes several subsystems (summarized within Figure 7) that are focused on

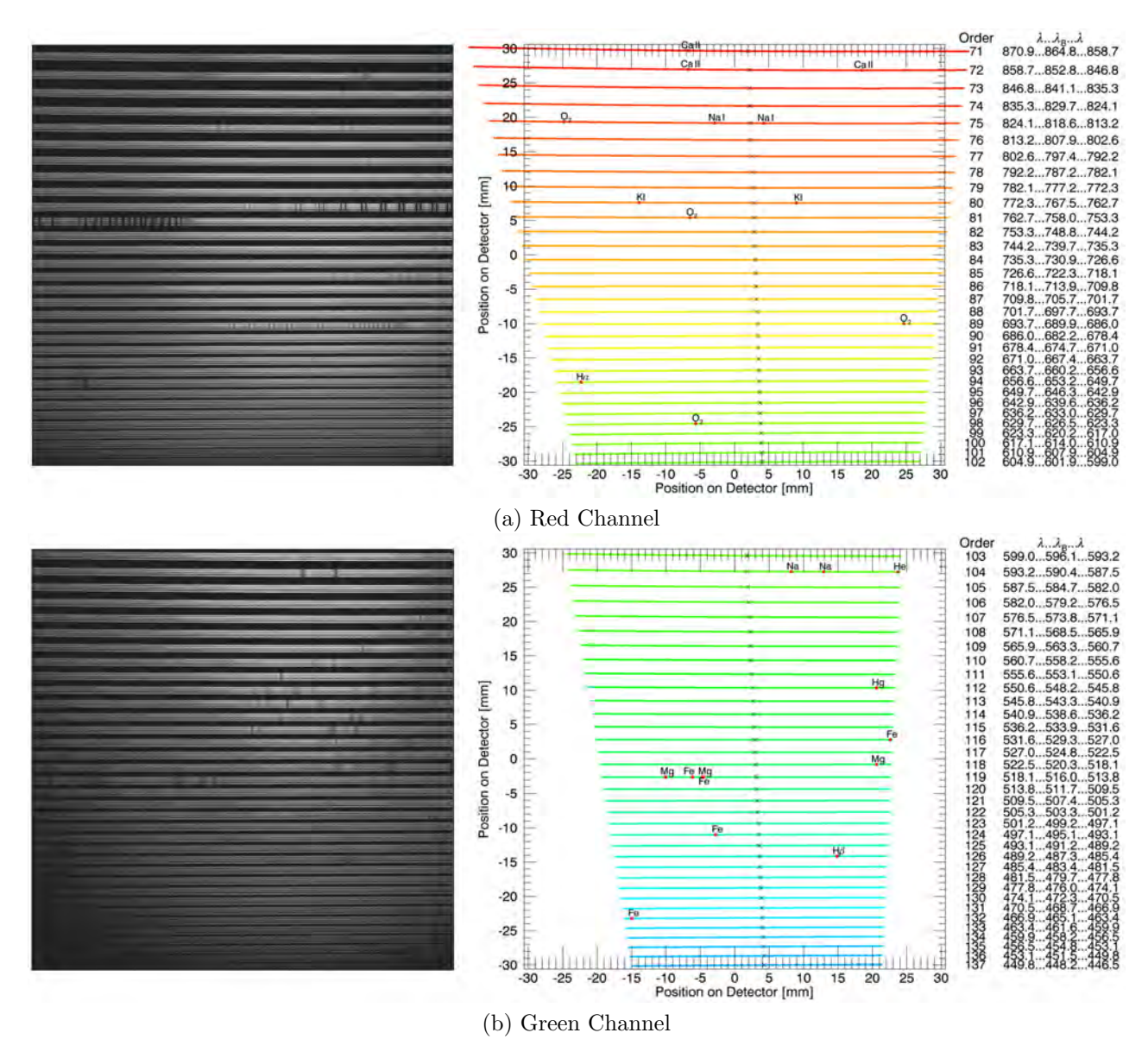


Figure 6. Left: KPF solar spectra from both channels. The SoCal subsystem (see Section 3.7.3) was used to collect and send light from the sun to the KPF science and sky fibers, and the Fabry-Pérot etalon was the source for the simultaneous calibration fiber. Right: Echellograms showing the orders for each channel out to one free spectral range, with Fraunhofer and other absorption lines of interest indicated.



Figure 7. Components of the KPF illumination homogenization system.

reducing the impact of sources of illumination instability. To ensure the designs performed adequately, the KPF optical fiber, agitator, and scrambler subsystems were thoroughly tested in the laboratory, with results presented in Sirk et al. (2018)<sup>11</sup> and Gibson et al. (2020).<sup>12</sup>

## 3.4.1 Fiber Injection Unit

Light from the Keck I telescope feeds the KPF Fiber Injection Unit (FIU), which is located on the adaptive optics (AO) bench on the Nasmyth platform. Note that KPF does not utilize the AO system for observations, however, the location is advantageous as the FIU is protected within a clean room, and it does not need to be re-positioned when KPF goes on-sky (only a small fold mirror translates into the beam to re-direct light from the telescope). This fold mirror also provides tip/tilt correction at 100 kHz, to stabilize the image at a level beyond what the telescope guiding system can provide.

The completed FIU (with super-imposed light paths) is shown in Figure 8. The FIU accepts the f/15 beam from the telescope and converts it to f/3.7 to minimize focal ratio degradation effects within the optical fibers. A pair of bandpass-selecting dichroics split the light bluer than 430 nm into a Calcium H & K arm (which sends near-ultraviolet light to the Calcium H & K spectrometer), and the remaining light bluer than 930 nm into a science arm (which sends light to the primary science fiber and two adjacent sky fibers which monitor contamination from the sky background). The FIU also includes an atmospheric dispersion corrector (ADC) for both the science arm (a pair of rotating prisms) and the Calcium H & K arm (the fibers are mounted on a 2-axis piezo-actuated translation stage). Near-infrared light beyond the KPF bandpass (and otherwise unused by the system) is sent to a guider arm which provides target acquisition and guiding. The FIU also offers a calibration mode, engaged when a small fold mirror translates into the beam, allowing light from two calibration system fibers to be re-imaged onto the main spectrometer's science and sky fibers for wavelength and flat-field calibration.

The FIU optical and mechanical design, as well as the control software, were the responsibility of WMKO (an ideal arrangement, as the FIU directly interfaces with the telescope itself and also with its guiding and control software). More details on the FIU are provided within Lilley et al. (2020)<sup>8</sup> and Lanclos et al. (2024).<sup>32</sup>

#### 3.4.2 Optical Fibers

Optical fibers are well known "scramblers", suppressing illumination changes at the fiber input (located at the telescope focal plane) to produce a more homogeneous output at the fiber output (located at the spectrometer). To improve the scrambling performance, the KPF science, sky and simultaneous calibration fibers have an octagonal cross-section. The use of optical fibers also allow for physical separation between the telescope and spectrometer, allowing the latter to be placed within a stable, gravity-invariant environment (such as within the observatory basement for KPF).

As shown within Figure 2, almost two dozen optical fibers of various lengths are used throughout the KPF system. For the main spectrometer fibers, we adopted a scheme of having separate fibers outside and inside of the vacuum chamber, with two dual-path lens-based scrambler systems (Section 3.4.4) allowing the light from the fibers to pass through the vacuum chamber wall. This approach has several advantages: one can replace the external fibers (if damaged) without opening the vacuum chamber; the alignment of the fibers with respect to the spectrometer is protected within the vacuum chamber (and therefore less likely to be disturbed); and the fibers are not bonded within a vacuum feedthrough which can increase focal ratio degradation.

For the octagonal cross-section and long-run fibers, each optical fiber was built up into a custom fiber cable assembly, with the fiber protected within 5-mm outer-diameter Miniflex PBT tubing<sup>12</sup> (similar designs have been adopted by other astronomical instruments<sup>36,37</sup>). While more than one optical fiber could have fit within each Miniflex tube; we placed a single fiber in each cable as this approach offered greater flexibility for fabrication,

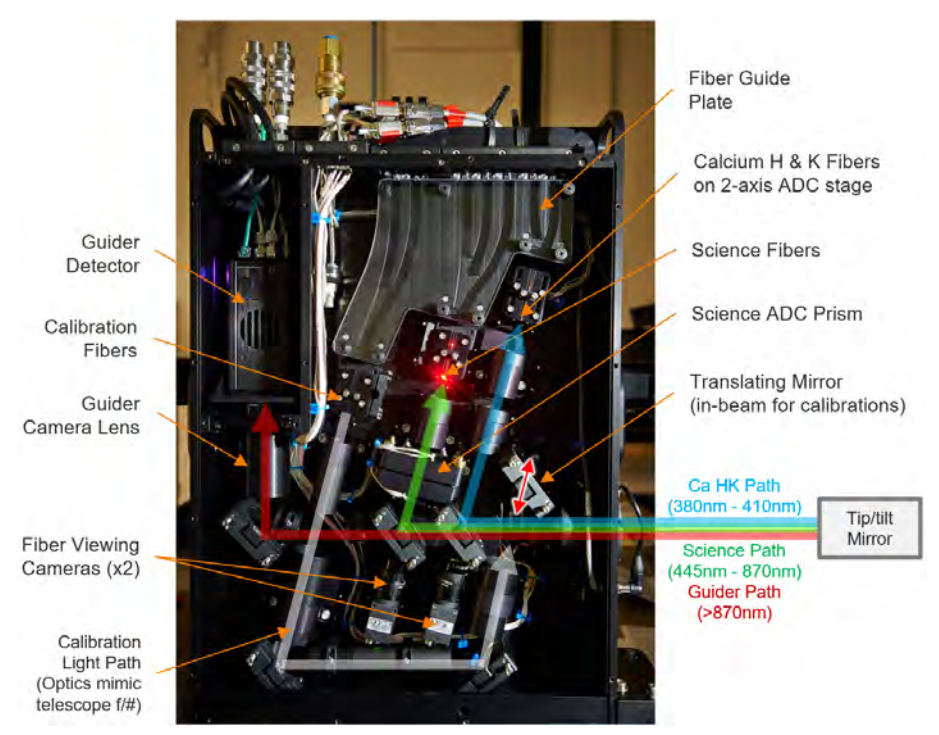


Figure 8. The KPF fiber injection unit with various features labelled. The bandpass provided by the telescope is split into the Calcium H & K, Science, and Guider bands by two dichroics (located where the green and blue paths reflect upwards). The gray line indicates the optical path for the calibration mode (engaged when a small fold mirror translates into the beam.

anti-reflection coating, installation, and maintenance/replacement operations. For the less-critical fibers (such as those within the calibration unit or the wideflat fiber systems), we used off-the-shelf Thorlabs patch cables.

A key driver for the science fiber was to keep its length as short as possible, as the system efficiency at the blue end of the green channel is especially affected by the internal transmission of this fiber. To this end, we determined the shortest fiber path possible from the FIU on the Nasmyth platform on the telescope to the spectrometer in the observatory basement (Figure 9). Once the shortest-practical path was determined (requiring 61 m of fiber), WMKO installed a new cable tray along this route, to enclose and protect the fiber cables as they negotiate the telescope structure and travel through the crypt and coudé tunnel to the basement.

To accommodate the telescope's azimuth rotations, a 1.9-m section of IGUS Triflex TRL-40-058-0 was installed to be coaxial with the axis of rotation, with one end connected to the rotating telescope and the other end to the fixed dome floor (the top end is shown at the right in Figure 9). As the telescope rotates through  $\pm 270$  degrees, this vertical, freely-rotating length of Triflex twists into a weak helix, within which the fiber cables follow an even-weaker helix as they are only loosely constrained by the Triflex internal sectors (each spanning 120 degrees). This torsional wrap design, being placed in-line with the fiber path, required no extra fiber length – a major advantage over the approximately 22 m of fiber that the existing cable wrap on the telescope would have required.

#### 3.4.3 Fiber Agitator

Fiber modal noise can also cause illumination instabilities at the output of a fiber <sup>38,39</sup> that limit the achievable signal-to-noise ratio, especially in a sliced beam. <sup>40</sup> To mitigate this effect, KPF employs a mechanical "agitator" to impose a periodic perturbation on the three fibers which feed the main spectrometer (the science, sky, and simultaneous calibration fibers). Within the KPF agitator (Figure 10), a section of each fiber cable is arranged into a pair of unequal loops, which are then tapped by two rotating bars causing the fiber loops to oscillate in multiple directions at several different frequencies. The result is that the paths of light through the fibers are

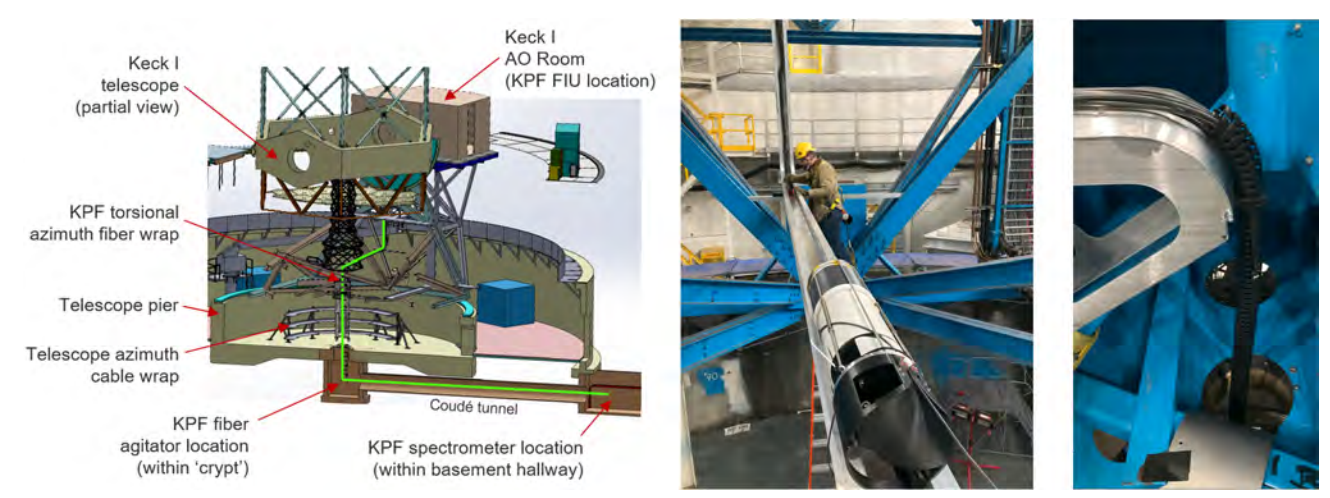


Figure 9. Left: Fiber path (in green) from the Keck I AO room (FIU location) to the observatory basement (spectrometer location). The telescope azimuth cable wrap is indicated, but was avoided through the use of a significantly smaller KPF-specific fiber wrap. Center: Installing the KPF fibers within the fiber trays mounted on the telescope. Within the vertical section a Triflex carrier can be seen; after the fiber cables were installed within it, the Triflex was twisted into a slow helix. This increased the internal friction in the fiber cables by adding a continuous weak bend, and was employed for the vertical sections of the route to prevent the optical fibers from sliding downwards within their protective tubing. In the foreground sits a spool of fiber cable waiting to be installed; these spools had to be custom-designed to pass the coiled-up fibers through the smallest aperture along the route. Right: The top end of the torsional fiber cable wrap which connects the rotating telescope to the fixed floor of the observatory.

constantly changing, which then homogenizes the fiber output over time. Tests performed with the prototype KPF agitator (reported in Gibson et al. (2020)<sup>12</sup>), found that modal noise was reduced to levels comparable to broadband light (the ideal) in under 4 seconds.



Figure 10. The KPF fiber agitator. Left: Front view showing the six fiber paths through the device. The science, sky and simultaneous cal fibers are agitated, and three backup copies of these fibers are also threaded through the agitator (but held away from the rotating bars). Right: A side view showing the rotating reel, which has two bars which tap the fiber loops. To minimize contact friction, the reel features PEEK tubing sections which independently roll as they contact each fiber cable.

#### 3.4.4 Fiber Scramblers

Each fiber path includes an additional scrambler,<sup>41</sup> consisting of a pair of doublet lenses,<sup>42</sup> that swap the near and far fields of the fiber output. The scrambler then feeds a short, 5 m length of octagonal fiber to further homogenize the scrambler output. Within the KPF scramblers, a vacuum window is placed between the lenses, allowing the scrambler system to double as a vacuum feedthrough for the main spectrometer vacuum chamber. The reader is directed to Gibson et al. (2020)<sup>12</sup> for more details on the KPF scrambler optical and mechanical designs.

# 3.5 Mechanical and Environmental Stability

In order to measure sub- $m s^{-1}$  Doppler shifts, it is critical for an EPRV spectrometer to exhibit a high level of mechanical and environmental stability. Three items designed to achieve this within the KPF system include the reformatter, the opto-mechanical design of the spectrometer, and the vacuum chamber system.

#### 3.5.1 Reformatter

Following the scramblers, the main spectrometer fibers end at the input to the reformatter. This system (Figure 11) takes the light leaving the science fiber, and rearranges it into three "slices", aligned along the spectrometer (virtual) slit. This offers an important mechanical stability advantage, as the reformatter allows the KPF spectrometer to be three times smaller than a traditional spectrometer that collects the same amount of flux and achieves the same resolving power. It also allows a large fiber to be used at the telescope focal plane (for increased efficiency through seeing-limited collection of starlight), while presenting the spectrometer with a narrow "slit width" (which allows high resolution).

Light from the science, sky, and simultaneous calibration fibers is incident on the reformatter, as shown at the left of Figure 11. A triplet lens magnifies the fiber outputs by a factor of eight and forms an image of the three fiber ends on the image slicing and masking mirrors. The science fiber image falls on three slicing mirrors, which then redirect the separate slices toward the pupil mirrors, which refocus the light to an intermediate image. The sky and simultaneous calibration fiber images are not sliced, but rather fall on separate masking mirrors on either side of the science-slicing mirrors. These fiber images also reach focus at the intermediate image via their own pupil mirrors. Through this combination of slicing and masking, all of the orderlets feature the same "slit" width in the spectral direction. The combined intermediate image is then de-magnified by a pair of relay mirrors, to form an f/8 image at the entrance slit position of the spectrometer.

As also shown within 11, two additional mirrors collect the light from the otherwise-unused outer edges of the science fiber, and send it to a fiber which travels to the exposure meter (Section 3.7.1).

The optical design of the reformatter is based on that shown in Vivès et al. 2016.<sup>44</sup> The KPF team worked closely with Winlight Systems during the design phases of this subsystem, after which Winlight fabricated the KPF reformatter (shown in Figure 12).

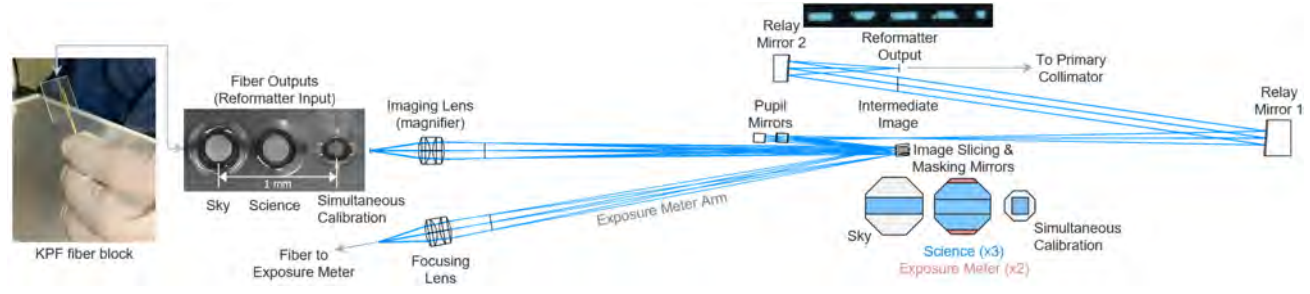


Figure 11. Optical design of the KPF reformatter. The inset at top right shows the image presented at the spectrometer slit location, with the science fiber sliced three times and the calibration and sky fiber outputs masked to have the same width in the spectral direction as the science slices. These five images are the sources for the five orderlets within each echelle order of a KPF spectrum. The fiber block at the reformatter input was manufactured by Femtoprint, and the fibers within were installed by the KPF team at SSL.

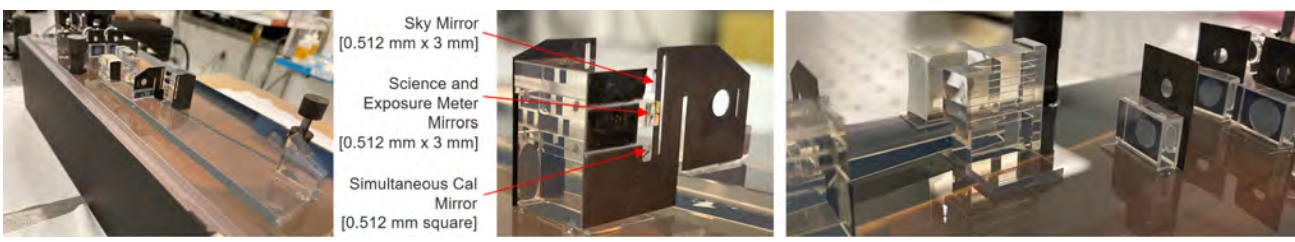


Figure 12. Pictures of the as-built KPF reformatter (fabricated by Winlight Systems). Left: To maximize stability with respect to temperature changes, the reflective optics within the reformatter are made of Zerodur, and are optically-contacted onto a Zerodur support base. <sup>43</sup> Note the Zerodur base sides were painted black to contain any stray light paths within the base. Not shown is a protective (and stray-light-suppressing) cover which sits within the depressed outer edge and is bolted to flexures (one of which is visible at the far right of image). Center: Close-up of the slicing/masking mirror stack. The black metal pieces featuring various apertures are stray light masks. Right: The pupil mirror stack is shown at the center of the image (with relay mirror 2 visible behind it). At far right sit several apertures for stray light suppression.

An important point to note is that the reformatter is illuminated with a stabilized source, as it is fed by the output of the entire illumination homogenization system (Figure 7). This is a very different situation than placing a traditional slicer at the focal plane of a telescope, where the illumination stability suffers from seeing and guiding issues. By placing the reformatter after the homogenization system, changes in illumination between each slice are reduced to negligible levels.

During the reduction of spectra, each science slice is treated independently as there are very small offsets in the wavelength solution between slices (these are impossible to remove completely, and were greatly minimized by Winlight's precision fabrication techniques). Therefore we do not simply collapse the three slices together, but rather treat each orderlet as an independent measurement during reduction.

# 3.5.2 Optical Bench and Optical Mounts

Stability analyses undertaken within Zemax demonstrated that nanometer-level movements of the main spectrometer optics cause spectral shifts at the 10 cm s<sup>-1</sup> level.<sup>45</sup> Within EPRV spectrometers such movements are typically constrained by exquisite milli-Kelvin (or better) temperature stability to minimize expansion and contraction effects (for example, HARPS<sup>28</sup> and HPF<sup>46</sup>). The KPF design approach was to minimize the effects of temperature changes or gradients by utilizing low coefficient of thermal expansion (CTE) materials throughout the spectrometer. Minimizing local optic movements that shift the beam vertically with respect to the bench was especially critical, as this is along the direction of echelle dispersion within the KPF design.

A unique aspect of KPF is the use of a Zerodur optical bench to support the spectrometer, as shown in Figure 13. Our bench source was a 2 m diameter by 0.4 m thick disk of Zerodur that was purchased for, but then not utilized by, a previous SSL project (Figure 14, top left). The primary advantage of a Zerodur bench is its small CTE value, and our particular disk has an extremely low CTE value (approximately  $0.000 \pm 0.004 \times 10^{-6} \text{ K}^{-1}$ ,

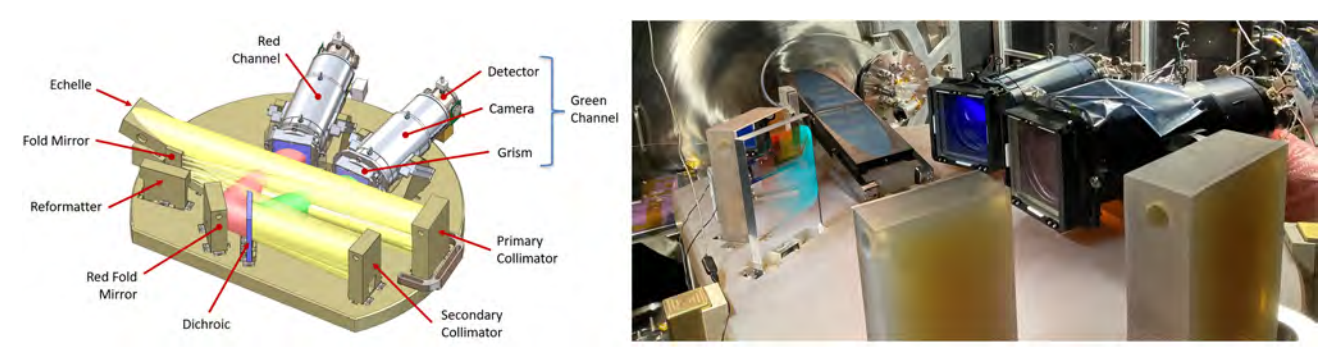


Figure 13. Left: The KPF spectrometer opto-mechanical design, with the optical elements supported by a Zerodur bench. Right: The fully-populated optical bench.

as measured by Schott). This CTE value is orders of magnitude smaller than metals typically used in optical benches (for example, it is 200× smaller than Invar 36 and 2940× smaller than Stainless 304).

The full Zerodur disk weighed 3177 kg and was too large in diameter to fit within the narrow hallway in the observatory basement (the preferred installation location for thermal stability reasons). Therefore, the disk was modified as summarized in Figure 14. Within Gibson et al.  $(2020)^{12}$  we discussed plans to acid-etch the bench pockets to relieve potential stress risers within the sub-surface damage layer that inevitably results from grinding processes. However, after discussions with Schott we instead moved to a finer abrasive size for final grinding of the pockets (from D64 to D46). This resulted in lower levels of induced sub-surface stress, and also offered a more uniform and controllable process than acid-etching the complicated geometries of the bench pockets.

Our overall opto-mechanical design approach was to take full advantage of the low-CTE bench by mechanically contacting optics and mounts - also made of Zerodur, where possible - to the Zerodur bench. Wherever possible, we specifically avoided high-CTE materials which are commonly used to mount optics (i.e. metals, RTV, plastics and epoxies).

The KPF optical mount design utilizes pockets machined into the top surface of the optical bench, as shown in Figure 14. Each optic sits within one of these pockets, with typically three vertical and three horizontal shim stacks used between the optic and the pocket walls (as shown in the left side of Figure 15). The optic is held in this location by spring force. With this method, there is only Zerodur between the optic (or mount) and the Zerodur bench, and the expansion and contraction of the metal springs cannot influence the position of the optic (rather only slightly affect the spring force they apply to the optic). Four springs are required for each optic: one vertical spring (to provide downward force against the shims in the pocket floor), and three horizontal springs (to provide sideways force against the shims contacting the pocket walls).

Details on the Zerodur shims are shown in Figure 15. There are two types of shims within each "shim stack"; one is flat-flat and one is flat-spherical. The single spherical surface compensates for tip/tilt differences between the bench and an optic (caused by either fabrication tolerances or deliberate alignment adjustments). One drawback, however, of the spherical contact is that it reduces the contact area and increases the contact

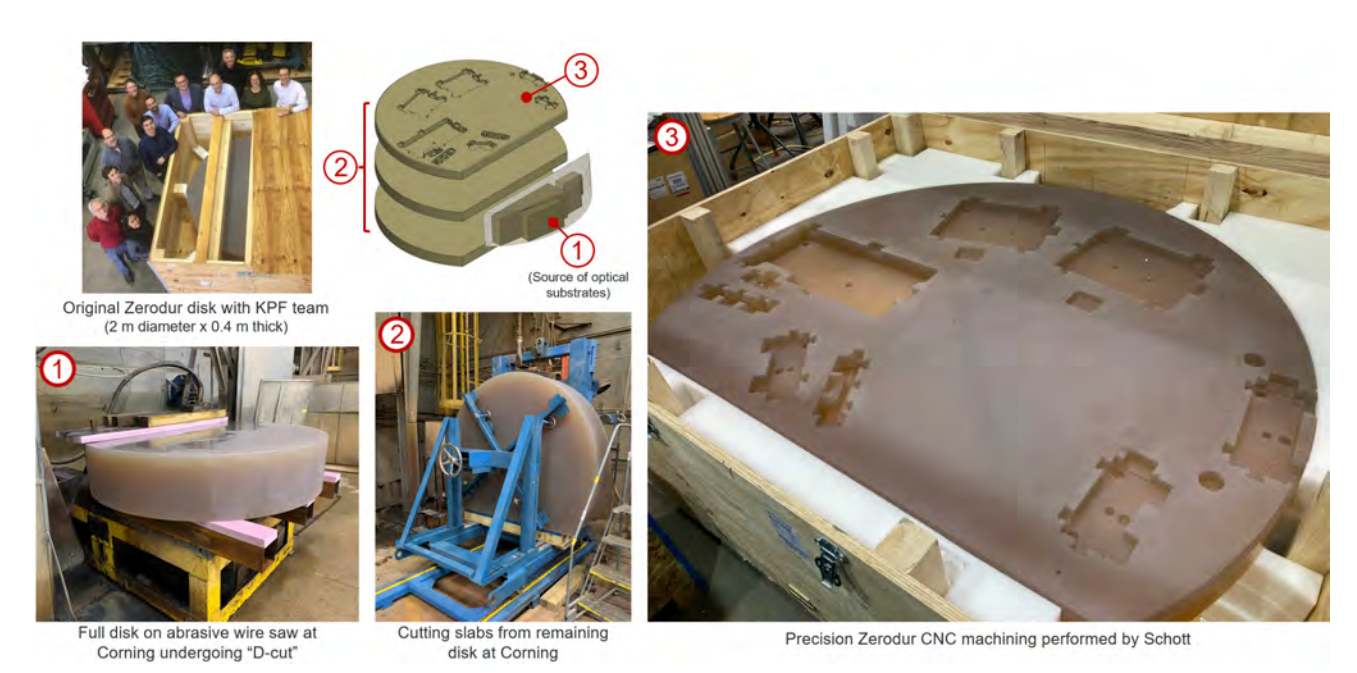


Figure 14. Fabrication stages of the Zerodur optical bench. Step 1: A "D-cut" was first cut from the disk, and this off-cut then became a source for several optical substrates. Step 2: The remaining large piece was then cut into three slabs. One of these became the final optical bench; a second was left as-is and reserved as a spare bench; and the third slab became a source for additional optical substrates. Step 3: The pockets for the various spectrometer optics were then CNC-machined into the bench.

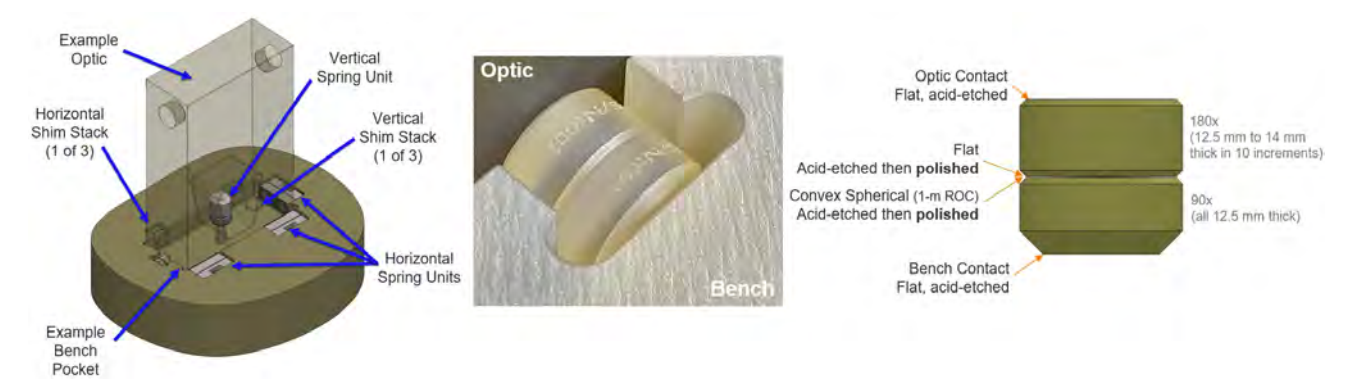


Figure 15. Mounting scheme and shim details. Left: Zerodur shims are used to register the optics against the Zerodur bench, with springs applying force to maintain the Zerodur-to-Zerodur contact. Center: A Zerodur shim stack installed within the spectrometer. Note that each shim has a serial number etched into its side for tracking shim lengths and placements. Right: Details of the shim stack design. As explained in the text, the central interface has one spherical surface to allow for tip/tilt adjustments.

forces at the interface. Therefore, to prevent potential damage to the optics or bench, the spherical surface was placed between the two (replaceable) shims. To increase stability, the shims were acid-etched on all sides to remove sub-surface damage from grinding operations, and the central spherical and flat contact surfaces were also polished. The intent here was to create a very strong and smooth surface so sub-surface damage would not collapse under the contact force. Finally, to aid assembly, shims of multiple thicknesses were purchased (see far right of Figure 15), which were then combined together as required during the alignment of the optics.

Examples of several as-built mounts are shown in Figures 16 and 17. The echelle and cameras required a slightly different mounting scheme, as they are located on the optical axis of the spectrometer (200 mm above the top surface of the bench), yet do not fully extend down to the bench. Given that mechanical stability in the vertical direction is key, these mounts were designed to place Zerodur between the bench and the optical axes of these optics. As such the echelle and camera mounts required two levels of shim-spring interfaces, as shown in Figure 17. For a more in-depth description of the KPF opto-mechanical design, the reader is directed to Smith et al. (2018).<sup>10</sup>

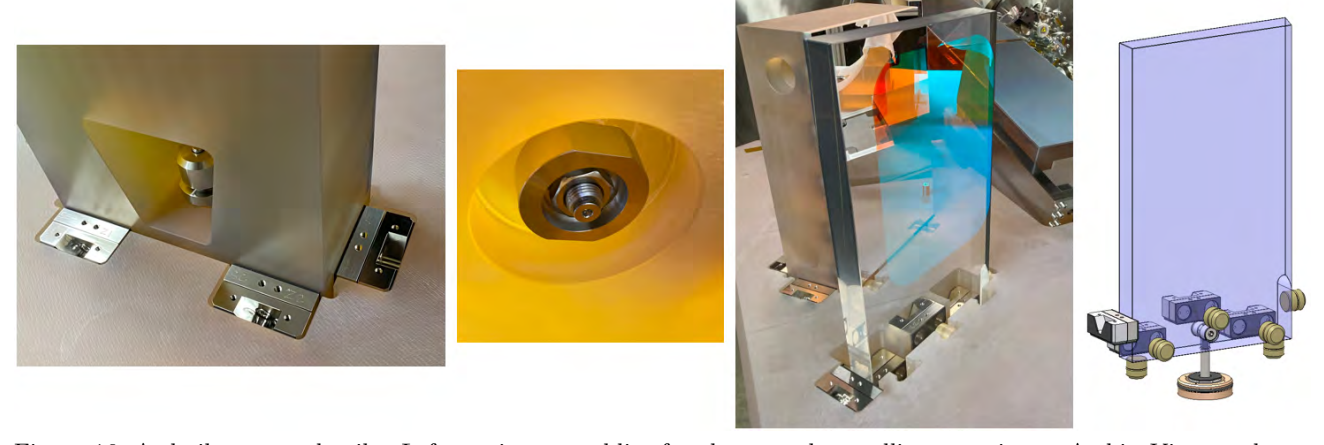


Figure 16. As-built mount details. Left: spring assemblies for the secondary collimator mirror. A thin Viton pad was installed on both sides of each spring, to provide a compliant interface between the stainless-steel spring mechanisms and the Zerodur bench and optics. Center-left: The bottom end of a vertical spring unit (viewed from under the bench). Center-right: the dichroic mounted within the bench. Right: Given the narrow width of the dichroic, a variation on the standard mount design was employed to maintain high stability. As shown, a deeper pocket was employed so that three shims could be placed on the front surface.

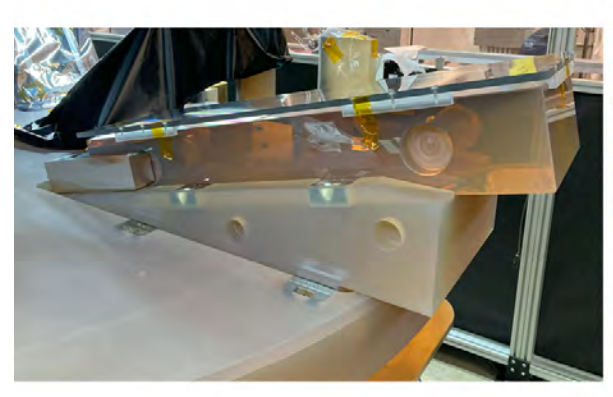




Figure 17. The echelle mount and the camera mounts feature two levels of shim-spring interfaces. Left: the wedge-shaped Zerodur echelle mount aligns the grating at its blaze angle (the echelle substrate is also Zerodur). Shown in this view are the springs at the bench-to-mount level, and the springs at the mount-to-echelle level. Right: The Zerodur camera fork-style mounts. The bench-to-mount shims are visible at the base of the foreground mount; the mount-to-camera shims are not yet installed, but are placed in pockets at the top of the fork arms. Machining of both the echelle and camera mounts was performed by Schott.

# 3.5.3 Vacuum Chamber and Optical Bench Support

In order to isolate the spectrometer from its environment, it was placed within a vacuum chamber (for isolation against convective thermal disturbances and changes in atmospheric pressure), and it will be surrounded by insulated walls in the observatory basement (for isolation against temperature changes). The thermal enclosure has not yet been installed, but installation is expected in late 2024 (see Section 4 for more details).

The KPF vacuum chamber design is shown within Figure 18. Two doors allow access to the interior; the doors feature articulating hinges to ensure a consistent and parallel pressure against the O-ring seal. To minimize the fiber length to the telescope, the two scrambler systems are located on the door closest to the coudé tunnel. Within the chamber, the optical bench is supported on five vacuum-compatible Minus K CM-1 isolators to prevent vibrations or chamber deflections from influencing the positions of optics on the bench. These isolators are supported on a platform sitting on eight wheels. The wheels allow for the spectrometer to be installed or removed from the vacuum chamber, and are mounted on adjustable eccentric cams to ensure wheel-to-track contact is maintained when the instrument is installed within the chamber.

The KPF system was initially assembled and tested at SSL. Prior to shipment to the observatory, the optics were removed from the bench. At the observatory, the optics were re-installed using a 2-axis bridge crane located just outside the vacuum chamber. The bench and support assembly were then rolled into the vacuum chamber as shown in Figure 18.

## 3.6 Calibration System

The KPF calibration system resides in the observatory basement hallway near the spectrometer. The core of the calibration system consists of off-the-shelf components (lenses, filters, beamsplitters, and fiber holders) mounted on a standard optical breadboard. To select between sources, we adopted the system developed by the CARMENES team, where the lamps and sources are radially located on the faces of an octagon mount. <sup>47</sup> An advantage of this design is that both the sources and the fibers remain stationary during source changes. To further select between various combinations of sources and fibers sending light to the spectrometer, several shutters are located throughout the system.

As was shown in Figure 2, two calibration fibers travel up to the telescope, where the FIU focuses the calibration light onto the science and sky fibers (for calibrations between science exposures). A third calibration

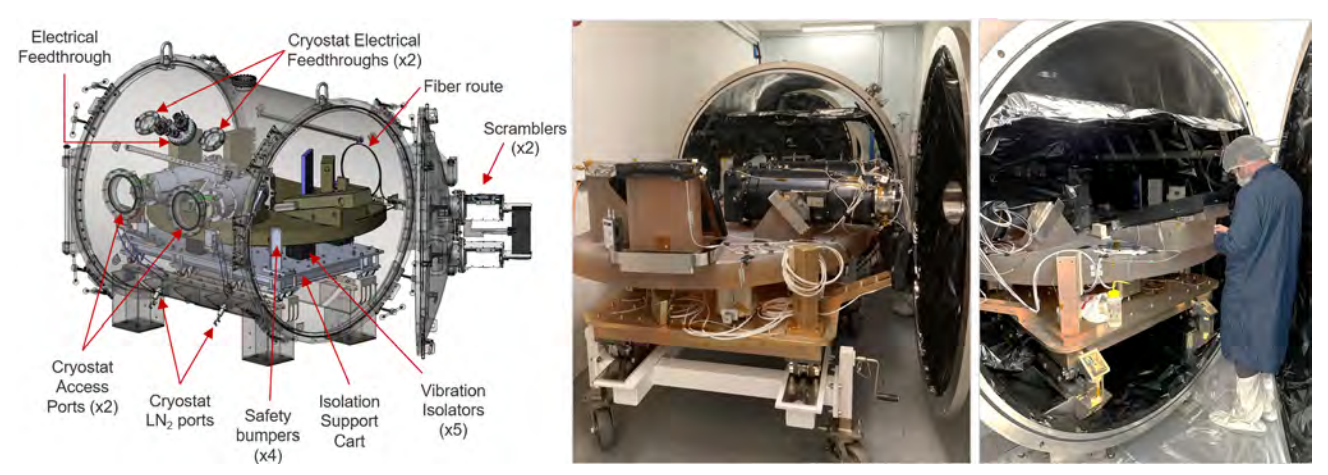


Figure 18. Left: The KPF vacuum chamber with main features labelled. The center section of the chamber is 1892 mm in diameter and 2045 mm long. The safety bumpers constrain excessive bench movement but are not in constant contact with the bench. Center: The assembled spectrometer ready to be rolled into the vacuum chamber. The bench sits upon five isolation pedestals (one of which is visible), which are attached to the bench support platform, which sits upon wheels which roll on tracks on the (white-painted) assembly cart. The various white cables are for temperature sensors. Right: The spectrometer installed within the chamber. Note the black MLI lining the chamber, which was used to thermally isolate the spectrometer from the chamber wall, and also to reduce stray light paths within the chamber.

fiber travels directly to the spectrometer to provide a simultaneous calibration source during a science exposure. Note that this simultaneous calibration fiber also passes through the agitator, to ensure that the modes within this smaller fiber are fully homogenized.

The system includes typical spectrometer calibration sources (Thorium-Argon and Uranium-Neon hollow-cathode lamps for wavelength calibration, and a broadband continuum source for flat-fielding), as well as a laser frequency comb (LFC) and a Fabry-Pérot etalon to provide high line density sources to track instrument drifts. The LFC (from Menlo Systems) provides stable, uniformly-spaced emission lines across the KPF bandpass that are traced to a fundamental frequency standard that is stable at the 10<sup>-14</sup> level. Operationally, the LFC is used minimally (to extend the lifetime of consumable parts within), and the etalon (built at Macquarie University) serves as the primary wavelength calibrator, providing a highly uniform comb of unresolved lines spanning the whole wavelength range of the spectrometer (at a spacing of three resolution elements at the bluest wavelengths). Rounding out the calibration system is the "wide flat" illumination system, which overfills the echelle orders for flat-fielding the entire CCD by providing diffuse illumination between the orderlets. Within the spectrometer, the output f/cone of the wide flat fiber is slowed by a plano-convex lens, selected so the wide flat beam just over-fills the echelle grating. This lens is located just above the reformatter output, and is suspended by an arm mounted on top of the intermediate fold mirror.

## 3.7 Ancillary Measurements

Several subsystems are included within the KPF system to provide contemporaneous ancillary measurements which complement the observations obtained with the main spectrometer. Described within this section, these subsystems include: the exposure meter (for barycentric corrections); the Calcium H & K spectrometer (for stellar activity monitoring; and the Solar Calibrator (a solar feed allowing daytime use of KPF on an astrophysical source).

# 3.7.1 Exposure Meter

An exposure meter is employed to determine the chromatic photon-weighted mid-exposure time of each observation, which is required to accurately determine the barycentric correction and account for the movement of the Earth during an observation. The KPF exposure meter is a prism-based, low-resolution ( $R \simeq 100$ ) spectrometer covering the main spectrometer bandpass. A spectrometer-based exposure meter allows the exposure mid-time calculation to account for chromatic effects including differential atmospheric refraction, variable atmospheric

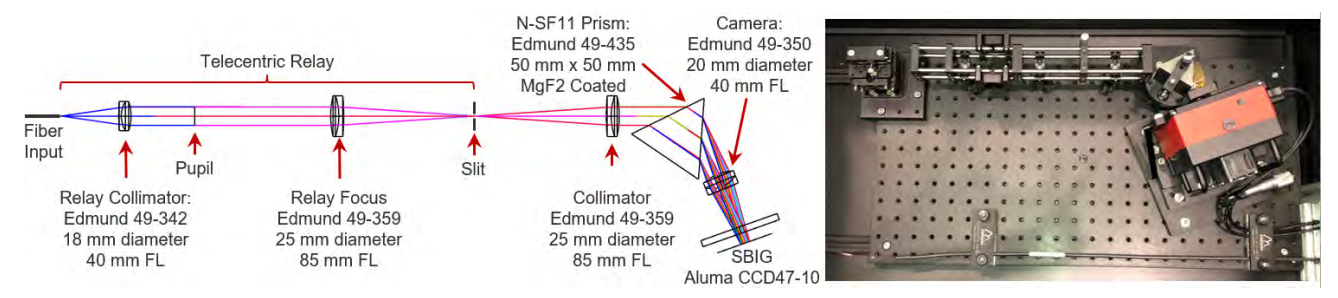


Figure 19. The optical design of the exposure meter and the as-built instrument.

attenuation as an exposure tracks a star across a changing airmass, and the chromatic performance of the guide system. The barycentric correction(s) can then be computed for multiple distinct wavebands spanning the spectrometer's bandpass. Analysis showed that the exposure meter could make the required measurement if it received 1% of the flux that the main spectrometer receives. This was achievable by collecting the light from the two otherwise-unused outboard slices on the science fiber face, as was shown in Figure 11. The exposure meter system can also be used to terminate an observation when a desired SNR is reached by the main spectrometer. The optical design and the as-built instrument are shown in Figure 19. More details on the optical and opto-mechanical designs of the KPF exposure meter are provided within Gibson et al. (2020).

## 3.7.2 Calcium H & K Spectrometer

A separate small spectrometer is used to monitor the Calcium H & K lines as indicators of stellar activity that could mimic Doppler shifts. An advantage of this approach is that the main spectrometer does not need to cover an increased bandpass blueward to 383 nm, resulting in several important advantages for the main spectrometer: smaller optical coating bandpasses and hence higher efficiencies; less complicated camera designs; and also smaller detectors. This spectrometer covers a bandpass of 383–402 nm (to include the Calcium H & K lines themselves and adjacent areas of the continuum) at a resolving power of R = 17,000. A throughput requirement of  $\geq 4\%$  was set to ensure that the Calcium H & K exposures do not take longer than the main spectrometer exposures. The Calcium H & K spectrometer is fed at the FIU by two fibers (Ca HK Science and Ca HK Sky), and is installed within the AO Electronics Room on the Keck I telescope. This location was chosen for throughput considerations, as it allowed for the shortest practical fiber length (10 m). The optical design and the as-built instrument are shown in Figure 20. A full description of this instrument is provided by Baker et al. (2022).

## 3.7.3 Solar Calibrator

The KPF Solar Calibrator (SoCal) provides a dedicated solar monitoring system that feeds KPF with stable, disc-integrated sunlight during the day. This 'Sun-as-a-star' dataset has proven extremely useful for assessing the performance of the instrument and data reduction techniques, and for gaining insight into the lowest-level activity signals across a wide range of timescales.<sup>54,55</sup>

The SoCal instrument is installed on the observatory roof within its own weatherized enclosure. A 75-mm diameter lens and 2-inch integrating sphere, mounted on an autonomous Sun-tracking mount, are used to collect

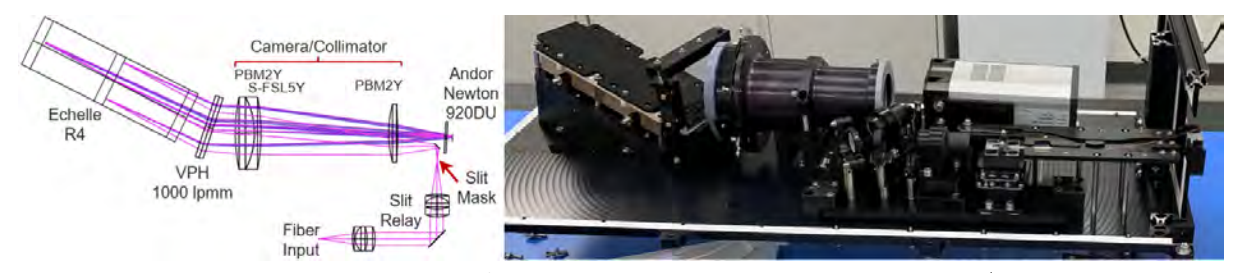


Figure 20. The optical design of the Calcium H & K spectrometer and the as-built instrument (with echelle grating cover in place). The larger camera lenses are 100-mm in diameter, and the R4 echelle grating measures  $70 \times 210 \,\mathrm{mm}$ .

disc-integrated sunlight (as shown in Figure 21). Weather permitting, upwards of  $\sim 350$  high signal-to-noise solar spectra are collected each day in the six-hour window between the standard KPF morning and evening calibration sequences. Signal-to-noise ratios of up to 2400 can be obtained in a 12 sec exposure. The cadence can be increased to  $\sim 800$  spectra per day by utilizing KPF's fast readout mode (with < 16 sec between exposures).

A key advantage of the SoCal instrument is that it maximizes use of KPF since instrument performance and stability can be tracked during daylight hours with an astrophysical source. This has proven extremely useful for identifying systematics, monitoring instrument drifts, and developing methods to mitigate stellar activity. It also allows a direct comparison to other EPRV instruments with solar feeds (NEID, EXPRES, HARPS, HARPS-N). SoCal data is publicly available on the Keck Observatory Archive (KOA) within one day of collection. The reader is directed to Rubenzahl et al. (2023)<sup>57</sup> for a more detailed description of the SoCal hardware, instructions for accessing the data, as well as a report on its preliminary on-sky performance.

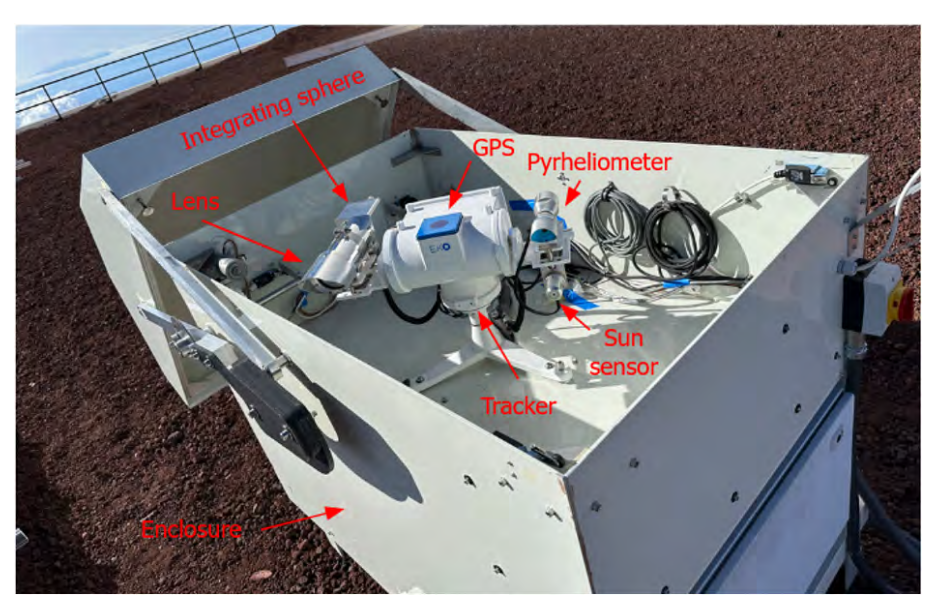


Figure 21. The KPF Solar Calibrator, with main components labelled. An EKO Instruments STR-22G mount, with an on-board sun sensor, provides automated solar tracking. On one arm of the EKO mount, a small lens creates an image of the solar disk at the entrance of the integrating sphere. After of order 1000 reflections within the integrating sphere, the light enters several 90-m long optical fibers, which carry the light to the KPF calibration unit and spectrometer in the observatory basement (see Figure 2). A pyrheliometer is mounted on the opposite arm and is useful for monitoring cloud cover. Finally, the instrument sits within a weatherproof enclosure (custom-made by Fornax Mounts) with a motorized roof which opens for observations.

# 3.8 Software

This section provides a brief summary of the software developed to monitor and control the instrument, and to reduce and analyze the spectra obtained during an observation.

## 3.8.1 Instrument Control Software

The KPF instrument control software (ICS) provides users with an interface to control (and to read telemetry from) the instrument and was developed and written by UCO. The ICS conforms with the Keck Task Library (KTL), a standard WMKO software component that is used in every instrument at the observatory. Two of KTL's notable features include the concepts of 'dispatchers' (which perform dedicated tasks, such as communicating with a device), and 'keywords' (which are used to store telemetry values or act as control variables for data shared between dispatchers).

Given the large number of subsystems within KPF, approximately two-dozen KTL dispatchers were written to interact with the various electronic devices. Additional dispatchers were also created to handle software-only

tasks, such as: assembling the various spectra and images together (Green, Red, Calcium H & K spectrometer, exposure meter, and guider), along with telemetry and header information, into a single FITS file following an observation; to record telemetry values into a database; to send alarms (via email or Slack) if critical telemetry falls outside of nominal values; to orchestrate the timing of the various shutter transitions and detector pre- and post-exposure routines to ensure the Green, Red, Calcium H & K spectrometer and exposure meter exposures are contemporaneous.

In addition, there is an extensive set of high level scripts\* written in Python, which interact with the KTL keywords to automate various tasks. Each script is actually a Python class which is invoked by an execute() method which itself calls the pre\_condition(), perform(), and post\_condition() methods. This three-part structure allows the script to check that the system is ready for the action to be performed, then execute the action, then confirm a successful execution. These scripts can also be invoked via a command line interface to the underlying python and are used for everything from small, atomic actions which might require only a single KTL keyword write to execute, to large scripts which need significant flow control such as executing a science observation at night – including configuring the instrument, waiting for the telescope and tip-tilt system to acquire the target, executing the specified exposures, and finally performing clean up actions.

#### 3.8.2 Data Reduction Pipeline

The KPF data reduction pipeline (DRP) automatically delivers publication-quality data to users through KOA. It is designed to be accurate, reproducible, and extensible. The pipeline is available as open-source code housed in a GitHub repository<sup>†</sup>, and supports both continuous integration and continued contributions from the community. The DRP functions within the Keck Data Reduction Pipeline Framework, which is a lightweight software ecosystem created to unify the processing of data from various instruments at WMKO. The core DRP is built upon 'recipes' within this framework for flexible execution on a variety of platforms (from laptops to supercomputers). This architecture allowed us to build on established algorithms while also giving developers the freedom to isolate and improve each module separately. The DRP is written with in python, with an object-oriented focus, extensive version control for increased robustness, segregated development, maintainability, and testing capability.

The DRP automatically produces three levels of data products<sup>‡</sup> broadly categorized as Level 0 (raw 2D images), Level 1 (processed 1D spectra), and Level 2 (high-level derived data products). Of most relevance to the majority of users, L2 derived data products will include cross-correlation functions, stellar activity metrics, telluric parameters, and RV measurements. All KPF science observations will be publicly available on KOA after a standard 18 month proprietary period. This will include raw spectra and publication-quality RVs produced automatically by the open-source DRP. Calibration data and solar observations<sup>57</sup> are immediately made public. Further details on the DRP architecture, algorithms, and performance will be described in an upcoming paper (Fulton et al. in prep).

# 4. SERVICING MISSIONS AND FUTURE PLANS

During February of 2024 we took the instrument off-sky for a period of three weeks to address several minor issues. These included: a slight re-alignment of the reformatter fiber block to improve the symmetry of the slices; a replacement of the cryostat ion pumps (a preventative measure as the original ones had seen many air-vacuum cycles during integration); a re-alignment of the wide flat fiber to better center its illumination pattern with respect to the echelle orders; adjustment of the position of the green camera to improve image quality across the field (resolving power was showing degradation at the blue end of each echelle order); and the etalon internal alignment was optimized to increase its output flux.

Although we do not undertake these interventions lightly (as they reset the instrument stability timeline), we have another one planned for late 2024. This second servicing mission will have two major objectives. The first is to install the thermal enclosure around the main spectrometer vacuum chamber. This enclosure was

<sup>\*</sup>https://github.com/KeckObservatory/KPFTranslator

<sup>&</sup>lt;sup>†</sup>https://github.com/Keck-DataReductionPipelines/KPF-Pipeline

<sup>&</sup>lt;sup>‡</sup>https://kpf-pipeline.readthedocs.io/en/latest/data\_exploration/start.html

planned from the very start of the KPF project, however, the COVID-19 pandemic and the resulting impact on manufacturing lead times meant major delays in quoting and fabrication. The second objective is to change the detector cooling system away from liquid nitrogen (LN2), as this has proven to be an operational issue for WMKO (LN2 supply dewars are not allowed in the WMKO basement for safety reasons, which has meant long - and inefficient - LN2 supply lines). As such we plan to change the cooling system over to a closed-cycle refrigerant (CCR) system, which will remove the LN2 safety concerns and the need for daily LN2 fills.

## 5. LESSONS LEARNED

As with any major project, there were some lessons learned, which we include here for the benefit of others:

- Zerodur Chamfers: To reduce machining time (and cost), we minimized the chamfers on the Zerodur bench pockets and on the echelle and camera mounts. During integration we regretted this decision, as larger chamfers would have helped to guide the optics into place, and have helped to reduce the risk of damage.
- Spare Substrates: Having spare substrates on-hand can allow for a quick recovery from a fabrication error. For example, we did not have a spare dichroic substrate, which meant we were forced to accept a coating that did not meet our requirements (as a time-intensive removal of the coating did not fit within our integration schedule or budget).
- Independent Systems: As mentioned above, we combined part of the CCD thermal control system with the CCD controllers. This has led to small thermal instabilities whenever the CCD controllers need to go offline (for example, to load a new configuration file). This could have been avoided if we had decoupled the systems and employed a dedicated thermal controller. Independent systems also lead to easier troubleshooting, as they can be individually power-cycled.
- Optical Breadboard Assemblies: The calibration unit is composed of off-the-shelf optics and mechanics, with the optics mounted on posts and clamped down on a standard optical breadboard. We underestimated how hard this assembly would be to align, and in retrospect should have spent more time designing custom opto-mechanics with more deterministic optical placements.
- On-sky Fiber Alignment: We planned to use a pair of fiber-viewing cameras within the FIU to ensure that the telescope was correctly aligning targets to our fibers. In practice however, ghosts and low-flux levels have limited the usefulness of these cameras. The cameras as-designed were also not able to verify the performance of the ADCs. As such we were forced to use the exposure meter for these optimizations, which proved to be time intensive and difficult to interpret as continually-changing seeing effects were included. We regret not including more direct diagnostics within the FIU to optimize fiber alignment and ADC performance.

#### 6. INITIAL PERFORMANCE RESULTS

At the time of writing, KPF has been on-sky and making science observations for over a year. The KPF team is currently working on a paper focused on the performance of the instrument, but within this final section we present a few highlights of the instrument's performance so far.

## 6.1 Resolving Power

The as-built resolving power has been measured at R = 95,000 - 97,000 (Figure 22), which provides rich spectral detail for Doppler shift measurements (Figure 23). The resolving power is remarkably uniform across the red channel. Initially on the green channel the resolving power at the blue end of each order showed a distinct down-turn. Investigations during the first servicing mission (Section 4) implied this was owing to a slight CCD tilt; we have partially corrected the error and plan to further correct the CCD tilt angle in the future.

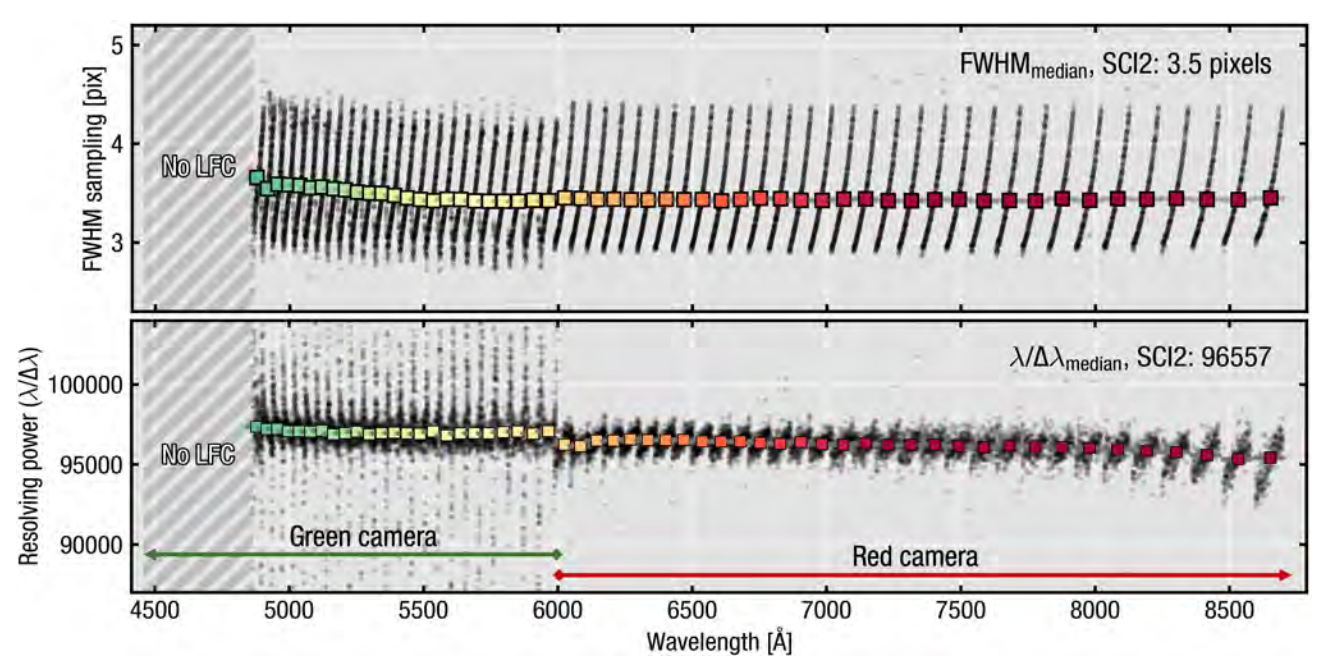


Figure 22. Achieved line-spread-function sampling (top) and spectral resolving power (bottom,  $R = \lambda/\Delta\lambda$ ) of the central KPF spectrometer science slice ('SCI2'), as measured using the broadband laser frequency comb (LFC) calibration source (the LFC does not currently produce usable lines blue-ward of ~4800 Å). Individual points (grey) are independent LFC line fits, parameterized by a gaussian + top-hat function, and colored squares show the order-by-order median values across the two KPF cameras. Across all three science channels, we reach R = 95,000 - 97,000, with a sampling of 3.4-3.7 pixels (full-width-half-max) in the dispersion direction.

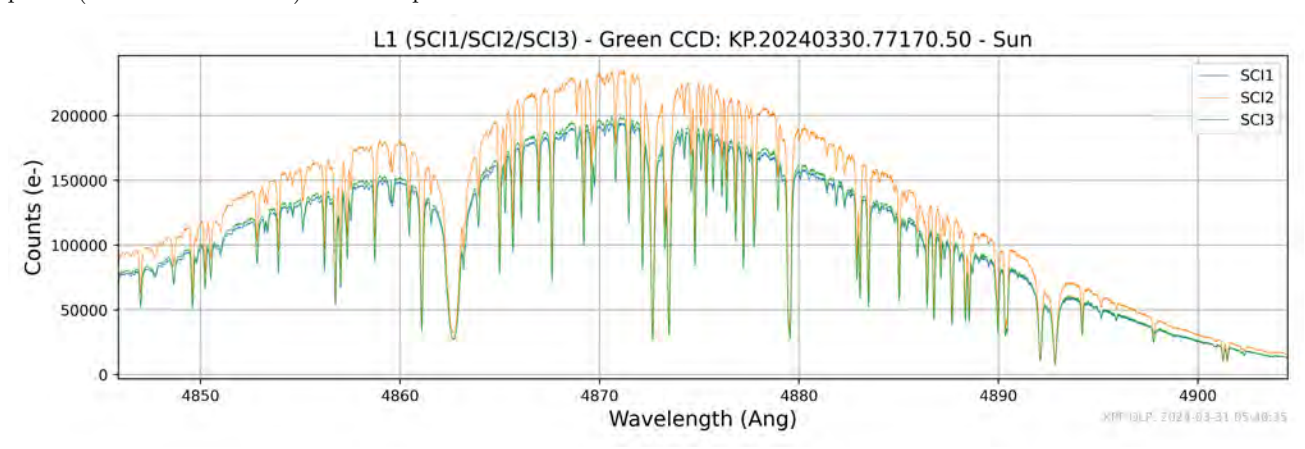


Figure 23. One echelle order trace from a KPF solar spectrum, showing the rich spectral detail available with the achieved resolving power of 97,000. The three traces correspond to the three orderlets generated from the science fiber by the reformatter. SCI2 is the central rectangular slice, which is slightly larger in area (and therefore contains more flux) than the two outboard SCI1 and SCI3 slices (which are trapezoidal in shape)

# 6.2 Instrument Throughput

Figure 24 shows the comparison between the instrument throughput model and a KPF observation of a spectrophotometric star (HR4554). The model includes atmospheric effects (such as atmospheric scattering/absorption at a Mauna Kea<sup>58</sup>), as well as all optical surfaces from the top of the telescope to the spectrometer CCDs (including all three science slices).

The overall shape of each channel is driven by the efficiency envelopes of the VPH gratings. The "dip"

between channels at approximately 600 nm is caused by the dichroic crossover region; unfortunately a coating deposition error on the dichroic substantially impacted throughput on the red side of the crossover region. The blue side of the green channel is affected by the preferential blue attenuation of the optical fibers, and the red side of the red channel is affected by the aluminum coatings on the Keck telescope primary, secondary, and tertiary mirrors.

With the exception of the blue end of the bandpass, the as-built instrument is out-performing the estimates of the (deliberately-conservative) efficiency model. The losses at the blue end remain a mystery to the team, but we are investigating the cause and hope to find a corrective solution.

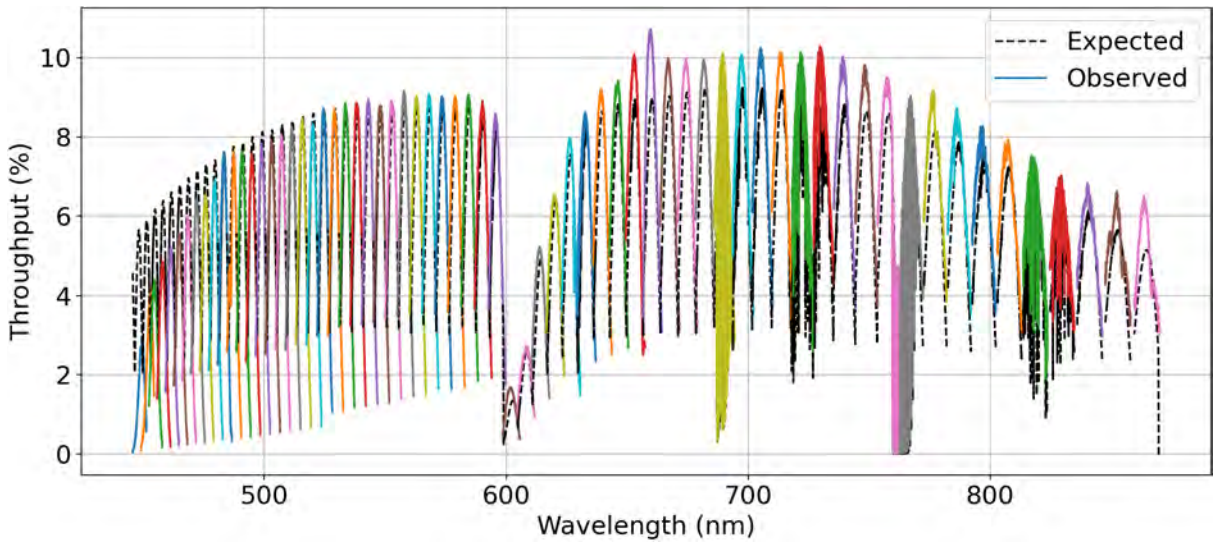


Figure 24. Total system throughput (top of atmosphere to detected photoelectron) estimated from KPF observation of HR4554 (Gamma Ursae Majoris), compared against the expected throughput curve from the KPF efficiency budget. The seeing during this observation was 0.58 arcseconds FWHM.

# 6.3 Instrumental Stability

As mentioned above, the KPF instrumental stability goal was set at  $30\,\mathrm{cm\,s^{-1}}$  for the residual, uncalibrated error due to the instrument and all subsystems. Figure 25 shows that KPF has surpassed this stability goal for most of the system error terms, with the raw unbinned data showing an internal instrumental drift of less than  $\sim 10\,\mathrm{cm\,s^{-1}}$  over the course of two weeks. The long term KPF on-sky and instrumental performance will be detailed in a future publication (Halverson et al., in prep.).

The primary limiting factor for long-term instrumental stability is the lack of a thermal enclosure surrounding the main spectrometer. After the installation of the thermal enclosure in late 2024, we expect an improvement in the stability of KPF over longer timescales as the spectrometer will be further isolated from its environment.

#### 7. SUMMARY

KPF has demonstrated state-of-the-art performance since delivery. The instrument has a high measured throughput ( $\sim 10\%$  peak in median seeing) and is now operating efficiently on Keck I. The Doppler stability of the instrument alone is at the level of  $< 10~{\rm cm\,s^{-1}}$  on weeks-long timescales, based on repeated observations of calibration spectra.

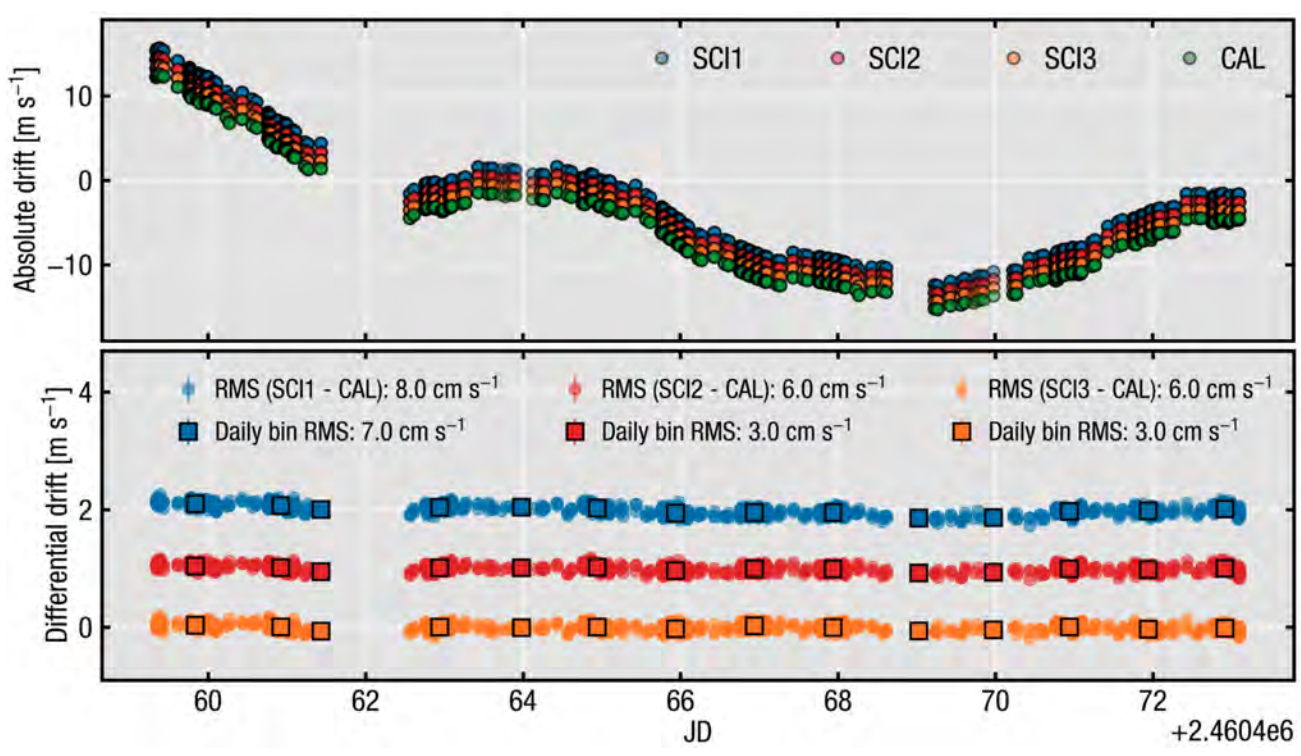


Figure 25. Sample KPF calibration RV time series spanning  $\sim \!14$  days. Data show all etalon calibration spectra collected (etalon illuminating all fibers at once) during this period taken during standard operation. For each quarter-night where KPF is not operating on-sky, a set of automated etalon spectra are recorded to monitor long-term instrument performance. Top: The absolute drift of the instrument (quantified in RV) for each of the individual fiber slices. Each slice time series is offset for clarity. The long term drift is driven by slow thermo-mechanical changes induced by multi-degree ambient temperature swings in the environment surrounding the vacuum chamber. We aim to significantly reduce these swings with the addition of a thermal enclosure (late 2024). Bottom: Post-calibration Doppler performance, assessed via measuring the differential drift of the three KPF slices of the science (SCI) fiber relative to the simultaneous calibration (CAL) fiber. The three slice (SCI1, SCI2, SCI3) time series are vertically offset for clarity. This achieved performance of 3-8 cm s<sup>-1</sup> differential RMS bounds a wide swath of terms in in the KPF error budget (Figure 1), and establishes that the bulk of the KPF system is contributing  $< 10 \text{ cm s}^{-1}$  systematic error over weeks-long timescales even in the presence of a significant absolute drift of the instrument.

#### ACKNOWLEDGMENTS

The authors thank the Heising-Simons Foundation, the National Science Foundation (award 2034278 through the Mid-Scale Innovations Program in Astronomical Sciences), private donors, the W. M. Keck Foundation, the Simons Foundation, the University of California, Berkeley, the California Institute of Technology, the University of Hawaii, the Jet Propulsion Laboratory, and the Mt. Cuba Astronomical Foundation for support of the KPF project. The authors also thank Winlight Systems for their valuable contributions to the designs of the reformatter and cameras and the DESI project for sharing their camera designs and their expertise with optical fibers. This research was carried out, in part, at the Jet Propulsion Laboratory and the California Institute of Technology under a contract with the National Aeronautics and Space Administration and funded through the President's and Director's Research & Development Fund Program.

## REFERENCES

- [1] Pepe, F. et al., "ESPRESSO at VLT. On-sky performance and first results," A&A 645, A96 (Jan. 2021).
- [2] Blackman, R. T. et al., "Performance verification of the extreme precision spectrograph," *The Astronomical Journal* **159**, 238 (apr 2020).
- [3] Schwab, C. et al., "Design of NEID, an extreme precision Doppler spectrograph for WIYN," *Proc. SPIE* **9908**, 99087H (Aug. 2016).
- [4] Cosentino, R. et al., "HARPS-N @ TNG, two year harvesting data: performances and results," 9147, 91478C (July 2014).
- [5] Seifahrt, A. et al., "On-sky commissioning of MAROON-X: a new precision radial velocity spectrograph for Gemini North," 11447, 114471F, SPIE (2020).
- [6] Crass, J. et al., "Extreme Precision Radial Velocity Working Group Final Report," arXiv e-prints, arXiv:2107.14291 (July 2021).
- [7] Gibson, S. R. et al., "Keck Planet Finder: Preliminary Design," 10702, 107025X, SPIE (2018).
- [8] Lilley, S. J. et al., "A fiber injection unit for the Keck Planet Finder: opto-mechanical design," 12184, 121844K, SPIE (2022).
- [9] Baker, A. D. et al., "A UV double pass spectrograph for monitoring stellar activity for the Keck Planet Finder," 12184, 121845H, SPIE (2022).
- [10] Smith, C. et al., "Keck Planet Finder: Zerodur optical bench mechanical design," *Proc. SPIE* **10702** (Aug. 2018).
- [11] Sirk, M. M. et al., "A optical fiber double scrambler and mechanical agitator system for the Keck planet finder spectrograph," 10702, 107026F, SPIE (2018).
- [12] Gibson, S. R. et al., "Keck Planet Finder: Design Updates," 11447, 1144742, SPIE (2020).
- [13] Howard, A. W. et al., "Planet Occurrence within 0.25 AU of Solar-type Stars from Kepler," *Astrophysical Journal Supplement* **201**, 15 (Aug. 2012).
- [14] Fulton, B. J. et al., "The California-Kepler Survey. III. A Gap in the Radius Distribution of Small Planets," Astronomical Journal 154, 109 (Sept. 2017).
- [15] Reiners, A. et al., "The CARMENES search for exoplanets around M dwarfs. High-resolution optical and near-infrared spectroscopy of 324 survey stars," A&A 612, A49 (Apr. 2018).
- [16] Batalha, N. E. et al., "The Precision of Mass Measurements Required for Robust Atmospheric Characterization of Transiting Exoplanets," Astrophysical Journal Letters 885, L25 (Nov 2019).
- [17] Winn, J. N. and Fabrycky, D. C., "The Occurrence and Architecture of Exoplanetary Systems," *Annual Review of Astronomy and Astrophysics* **53**, 409–447 (Aug. 2015).
- [18] Albrecht, S. et al., "Obliquities of Hot Jupiter Host Stars: Evidence for Tidal Interactions and Primordial Misalignments," ApJ 757, 18 (Sept. 2012).
- [19] Tabernero, H. M. et al., "ESPRESSO high-resolution transmission spectroscopy of WASP-76 b," A&A 646, A158 (Feb. 2021).
- [20] Beck, P. G. et al., "Fast core rotation in red-giant stars as revealed by gravity-dominated mixed modes," Nature 481, 55–57 (Jan. 2012).

- [21] Silva Aguirre, S. et al., "Ages and fundamental properties of Kepler exoplanet host stars from asteroseismology," MNRAS 452, 2127–2148 (Sept. 2015).
- [22] Boyajian, T. S. et al., "Stellar Diameters and Temperatures. II. Main-sequence K- and M-stars," ApJ 757, 112 (Oct. 2012).
- [23] Halverson, S. et al., "An Efficient, Compact, and Versatile Fiber Double Scrambler for High Precision Radial Velocity Instruments," ApJ 806, 61 (June 2015).
- [24] Halverson, S. et al., "A comprehensive radial velocity error budget for next generation Doppler spectrometers," 9908, 99086P (Aug. 2016).
- [25] Podgorski, W. et al., "A novel systems engineering approach to the design of a precision radial velocity spectrograph: the GMT-Consortium Large Earth Finder (G-CLEF)," *Proc. SPIE* **9147**, 91478W (July 2014).
- [26] Quirrenbach, A. et al., "CARMENES: an overview six months after first light," 9908, 990812, SPIE (2016).
- [27] Ben-Ami, S. et al., "The optical design of the G-CLEF Spectrograph: the first light instrument for the GMT," 10702, 107029K, SPIE (2018).
- [28] Mayor, M. et al., "Setting New Standards with HARPS," The Messenger 114, 20–24 (Dec. 2003).
- [29] Mahadevan, S. et al., "The Habitable-zone Planet Finder: A status update on the development of a stabilized fiber-fed near-infrared spectrograph for the for the Hobby-Eberly telescope," Proc. SPIE 9147, 91471G (July 2014).
- [30] Roy, A. et al., "Precision velocimetry planet hunting with PARAS: current performance and lessons to inform future extreme precision radial velocity instruments," **9908**, 99086R, SPIE (2016).
- [31] Gibson, S. R. et al., "KPF: Keck Planet Finder," Proc. SPIE 9908, 990870 (Aug. 2016).
- [32] Lanclos, K. and Walawender, J., "Keck planet finder tip/tilt control," Software and Cyberinfrastructure for Astronomy VIII 13101-163, Proc. SPIE (2024).
- [33] Queloz, D. et al., "The Fiber-Fed Spectrograph, a Tool to Detect Planets," in [IAU Colloq. 170: Precise Stellar Radial Velocities], Astronomical Society of the Pacific Conference Series 185, 13 (1999).
- [34] Perruchot, S. et al., "Higher-precision radial velocity measurements with the SOPHIE spectrograph using octagonal-section fibers," **8151** (Sept. 2011).
- [35] Avila, G., "FRD and scrambling properties of recent non-circular fibres," *Proc. SPIE* **8446**, 84469L (Sept. 2012).
- [36] Poppett, C. et al., "The DESI fiber system," 10702, 107027O, SPIE (2018).
- [37] Saviauk, A. et al., "Final design of optical fibre routing for 4MOST," 10706, 107065Y, SPIE (2018).
- [38] McCoy, K. S. et al., "Optical fiber modal noise in the 0.8 to 1.5 micron region and implications for near infrared precision radial velocity measurements," *Proc. SPIE* **8446**, 84468J (Sept. 2012).
- [39] Plavchan, P. P. et al., "Precision near-infrared radial velocity instrumentation II: noncircular core fiber scrambler," *Proc. SPIE* **8864**, 88640G (Sept. 2013).
- [40] Mahadevan, S. et al., "Suppression of Fiber Modal Noise Induced Radial Velocity Errors for Bright Emission-line Calibration Sources," ApJ 786, 18 (May 2014).
- [41] Hunter, T. R. and Ramsey, L. W., "Scrambling properties of optical fibers and the performance of a double scrambler," *PASP* **104**, 1244–1251 (Dec. 1992).
- [42] Avila, G. et al., "Performances of HARPS and FEROS fibers in La Silla ESO Observatory," *Proc. SPIE* **5492**, 669–676 (Sept. 2004).
- [43] Vivès, S. et al., "New technological developments in integral field spectroscopy," Proc. SPIE 7018, 70182N (July 2008).
- [44] Vivès, S. et al., "A set of Zemax user-defined surfaces to model slicer mirrors," Proc. SPIE 6273 (2006).
- [45] Gibson, S. R., "Tolerancing a radial velocity spectrometer within Zemax," *Proc. SPIE* **9911**, 991190 (June 2016).
- [46] Stefánsson, G. K. et al., "Ultra-stable temperature and pressure control for the Habitable-zone Planet Finder spectrograph," Proc. SPIE 9908 (2016).
- [47] Quirrenbach, A. et al., "CARMENES instrument overview," Proc. SPIE 9147, 91471F (July 2014).
- [48] Probst, R. A. et al., "A laser frequency comb featuring sub-cm/s precision for routine operation on HARPS," 9147, 91471C (July 2014).

- [49] Schwab, C. et al., "Rubidium traced etalon wavelength calibrators: towards deployment at observatories," *Proc. SPIE* **10702** (Aug. 2018).
- [50] Schwab, C. et al., "Stabilizing a Fabry-Perot Etalon Peak to 3 cm s<sup>-1</sup> for Spectrograph Calibration," *PASP* **127**, 880 (Sept. 2015).
- [51] Stürmer, J. et al., "Rubidium-traced white-light etalon calibrator for radial velocity measurements at the cm s<sup>-1</sup> level," Journal of Astronomical Telescopes, Instruments, and Systems 3, 025003 (Apr. 2017).
- [52] Landoni, M. et al., "ESPRESSO front end exposure meter: a chromatic approach to radial velocity correction," *Proc. SPIE* **9147** (Aug. 2014).
- [53] Blackman et al., "Accounting for Chromatic Atmospheric Effects on Barycentric Corrections," ApJ 837, 18 (Mar. 2017).
- [54] Collier Cameron, A. et al., "Three years of Sun-as-a-star radial-velocity observations on the approach to solar minimum," MNRAS 487, 1082–1100 (July 2019).
- [55] Klein, B. et al., "Investigating stellar activity through eight years of Sun-as-a-star observations," arXiv e-prints, arXiv:2405.12065 (May 2024).
- [56] Zhao, L. L. et al., "The Extreme Stellar-signals Project. III. Combining Solar Data from HARPS, HARPS-N, EXPRES, and NEID," *The Astronomical Journal* **166**, 173 (Oct. 2023).
- [57] Rubenzahl, R. A. et al., "Staring at the sun with the Keck Planet Finder: An autonomous solar calibrator for high signal-to-noise sun-as-a-star spectra," *Publications of the Astronomical Society of the Pacific* **135**, 125002 (dec 2023).
- [58] The Nearby Supernova Factory et al., "Atmospheric extinction properties above Mauna Kea from the Nearby SuperNova Factory spectro-photometric data set," A&A 549, A8 (2013).